

ABSTRACT

Title of Thesis: DESIGN AND TESTING OF A HIGH-POWER PNEUMATIC
EXOSKELETON

Joshua T. Geating, Master of Science, 2018

Thesis Directed By: Professor Norman M. Wereley

Department of Aerospace Engineering

A pneumatic ankle exoskeleton is designed, constructed, and tested to study the use of pneumatic artificial muscles (PAMs) and force sensitive resistors (FSRs) for increased running and jumping performance. PAMs are selected for their low weight, high power density, and natural compliance, all advantageous for exoskeleton applications. FSRs are selected as they can be packaged between the sole of the wearer's foot and a ground plate, enabling toe push-off force to be measured. Toe force measurement is an uncommon parameter to be measured on most lower extremity exoskeletons. A closed loop force controller is implemented using the FSRs as an input force and a strain sensor embedded in the PAM as the feedback sensor. This architecture is shown to achieve a high bandwidth, capable of following trajectories similar to that of a running gait or jumping force profile. The FSRs are shown to exhibit low hysteresis and high dynamic response, and moderate linearity compared to traditional strain gauge based transducers (SGBTs). Special attention is given to keep the structure realistically lightweight, as well as select and characterize sensors that could be realistically packaged in an end-use application.

DESIGN AND TESTING OF A HIGH-POWER PNEUMATIC EXOSKELETON

By
Joshua T. Geating

Thesis submitted to the Faculty of the Graduate School of the
University of Maryland, College Park, in partial fulfillment
of the requirements for the degree of
Master of Science
2018

Advisory Committee
Professor Norman M. Wereley, Chair
Professor Craig R. Carignan
Professor Axel Krieger

Table of Contents

Table of Contents	ii
List of Figures	iv
List of Tables	v
Chapter 1 - Introduction.....	1
1.1 Background, State of the Art	1
1.2 Objective of Present Research	4
1.3 Overview of Thesis	5
Chapter 2 - Exoskeleton Design and Fabrication	6
2.1 Requirements Development.....	6
2.2 System Level Controller Design.....	7
2.3 Mechanical Design	9
2.3.1 System Level Mechanical Overview	9
2.3.2 Actuation Technology Trade	10
Pneumatic vs. Electric.....	10
Pneumatic vs. Hydraulic	11
Pneumatic vs. Minority Actuation Technologies.....	12
Pneumatic PAM vs. Pneumatic Cylinder vs. Pneumatic Rotary Vane Actuator..	12
2.3.3 PAM Design.....	13
Power source, fielded endurance estimate	16
2.3.4 Exoskeleton Structural Design.....	18
PAM Interface.....	18
Carbon fiber rods and rod replacements	19
Side interface plates	20
Ankle Brace	21
Ankle Bearings.....	22
Lever Arm Plates	22
Toe/Ground Plate	22
2.4 Electrical, Proprioception Design.....	23

2.4.1 System Level Electrical Overview.....	23
2.4.2 Actuator Control Scheme.....	25
2.4.3 Proprioception Development	25
Applied Toe Force Sensor	26
PAM Force Sensor	27
Ankle Encoder	30
Weight Plate.....	31
Chapter 3 - Sensor Qualification and Characterization	33
3.1 Weight Plate Qualification.....	33
3.2 Toe Force Sensor Qualification	33
3.2.1 PAM Force Sensor Calibration	37
3.2.2 Ankle Encoder Calibration.....	38
Chapter 4 - System Control and Testing, Discussion	39
4.1 Control	39
4.2 Testing	40
4.3 Discussion.....	44
Chapter 5 - Conclusions, Future Work	48
5.1 Conclusions.....	48
5.2 Future Work	49
Appendix A - Source Code	51
Arduino Source Code.....	51
Matlab Source Code.....	55
Appendix B - Hybrid PAM Concept	56
Appendix C - Mechanical Drawings.....	57
References.....	72

List of Figures

Figure 1. Force Control Diagram.....	8
Figure 2. CAD Rendering of Ankle Exoskeleton.....	9
Figure 3. Side View of Ankle Exoskeleton.....	13
Figure 4. Theoretical PAM Force vs. Deflection vs. Pressure Curves.....	14
Figure 5. PAM Cross Section.....	16
Figure 6. FEA results.....	20
Figure 7. Bronze Hardstop.....	21
Figure 8. Control Electronics.....	24
Figure 9. Exoskeleton and packaged electronics.....	24
Figure 10. PAM Control Chain.....	25
Figure 11. Commercial FlexiForce Sensors Integrated on Toe Plate.....	27
Figure 12. PAM SGBT Spring Element Cross Section (units are in inches).....	28
Figure 13. Assembled PAM SGBT.....	30
Figure 14. RM08 Encoder and Shaft Magnet.....	31
Figure 15. Weight plate showing button load cells (Left) and upper plate installed (Right).....	32
Figure 16. FSR output force versus actual load.....	34
Figure 17. Testing FSRs integrated onto exoskeleton.....	35
Figure 18. Processed FSR signals versus weight plate signal.....	37
Figure 19. Detailed Controller Block Diagram.....	39
Figure 20. Control Input Response to Finger Pressing.....	41
Figure 21. 5 Hz Sine Wave PAM Response.....	42
Figure 22. 1 Hz Square Wave PAM Response unfiltered (left), 5 sample mean filter (right).....	43
Figure 23. LS-V25s Mass Flow vs. Outlet Pressure.....	46

List of Tables

Table 1. Overview of Ankle Exoskeletal Systems.....	2
Table 2.1 System Requirements vs. Final Capability.....	7
Table 2. Components Used for Strain Gauge Transducer Fabrication	30
Table 3. Contributors to Control Bandwidth Response	44

Introduction

1.1 Background, State of the Art

Lower extremity exoskeletons have been the focus of much research and development in recent years. They hold promise for a variety of applications, largely in the medical industry as well as for military and industrial use. These exoskeletons fall into three categories: rehabilitation for injury recovery, weight offloading of large packs or tools, and reduction in the metabolic cost of locomotion. Each of these categories prioritizes different design aspects, as dictated by the objective at hand. Rehabilitative exoskeletons systems such as [1] are typically focused on exerting relatively high forces in a very controlled manner, usually not exceeding a bandwidth of 1 Hz. Military offloading mechanisms such as HULC [2] are focused on reacting heavy loads into the ground through the exoskeleton structure, and typically have at least six degrees of freedom (DOF) including the hip, knee and ankle of both legs. They operate at the pace of a typical human walking gait. They are usually partially or fully passive, i.e. unactuated, meaning they produce no net positive work. A limited number of active systems such as XOS2 [3] contain actuators to augment the wearer's force, and require an off-board power source. They are fairly bulky and unable to perform dynamic tasks such as running and jumping. Lastly, exoskeletons such as [4] focus on reducing the metabolic cost of locomotion and bridge the gap between military and medical use. Some are focused on injury recovery, whereas others are intended to eventually become commercial products that decrease the energy required to walk and run [5]. These exoskeletons input energy on each stride, allowing the wearer to exert less force during

the push-off phase of a given gait. Table 1 outlines some of the most well known ankle exoskeleton developments.

Table 1. Overview of Ankle Exoskeletal Systems

Institution / Name	Classification	Actuated DOFs per side of body	Application Notes
University of Michigan [6]	Metabolic Cost Reduction	1 DOF Passive Clutch	Uses a custom mechanical clutch to store and release energy from a spring
University of Michigan [1]	Metabolic Cost Reduction	1 DOF Pneumatic artificial muscle	Uses on-off switch in foot to trigger low force pneumatic muscle
Raytheon – XOS 2 [3]	Military / Industrial	12 DOF Hydraulic	For use on military bases lifting etc. High force and speed capability. Large, requires off-board power.
U of C , Berkeley – HULC [2]	Military / Industrial	1 DOF Hydraulic Assist (+2 passive)	For reducing metabolic cost of carrying loads on back
Humotech [5]	Metabolic Cost Reduction	1 DOF Cable transmission	Off-board servo motor pulls a cable, which exerts a torque about the ankle
Carnegie Mellon University [7]	Metabolic Cost Reduction	1 DOF Cable transmission	Predecessor to Humotech exoskeleton. Also utilizes off-board servo motor
Massachusetts Institute of Technology [8]	Metabolic Cost Reduction	1 DOF Electric motor winch	Low force brushless motor reduces metabolic cost of walking
Yaskawa Ankle Walking Assist Device [9]	Therapy / Rehabilitation	1 DOF Electric motor	Intended for rehabilitation of strain-related injuries for the elderly
Ghent University, WALL-X [10]	Metabolic Cost Reduction	1 DOF Pneumatic artificial muscle	For reducing metabolic cost of walking. Uses learning algorithms to adjust pressure vs. stride

Though these systems span a wide range of technologies and applications, none are focused on operation at both high speed *and* high force. That is, ground reaction forces exceeding 1g and speeds matching that of an aggressive running gait (3 Hz). For untethered systems, these two regimes have been mutually exclusive thus far. The closest of the three categories are metabolic cost reduction exoskeletons, which are also designed to be lightweight and low impedance, but focus more on assisting the wearer rather than amplifying his or her physical prowess. As such, exerted torques for these systems do not

exceed that of 1g and are actuated in an open-loop fashion, i.e. the output forces are predetermined as a function of the stride position.

This is not without reason, however, as moving to this regime brings on complications. Using metabolic cost reduction exoskeletons as a baseline, increasing the force does two things. First off, power increases linearly with force as speed remains constant, given by the Equation 1.

$$P(t) = \mathbf{F} \cdot \mathbf{v} \quad (1)$$

Therefore, doubling the force output would double the power consumption. This would require the entire actuation powerchain to be upsized proportionally. In the case of an electric motor, this would mean a higher output battery, larger motor controller, and substantially larger motor. For pneumatic and hydraulic systems, the power source (pump, compressor, compressed air vessel) must allow a higher fluid output volume, the valves must utilize larger orifices, and the actuators must increase. This would also result in lower endurance for the same initial amount of stored energy. Secondly, the structure must be designed to withstand the larger forces. While this may seem like a trivial hurdle overcome by adding a small amount of mass to the structure, it is not so straightforward. Most exoskeletons designed for running speeds take advantage of the leg anatomy and wearer's shoe, attaching to the calf and/or shoe sole. Typically, either the tibia is used as a compressive loading element, or the shin has a lateral load reacted into it to balance the applied ground force. As force increases, however, it is unsafe to use the wearer's bone structure to react applied loads. Instead, care must be taken to ergonomically interface to the wearer's lower leg and exert an uniform force in the direction of the net force vector.

Some of these challenges are more resolvable than others and will be addressed in the following section.

1.2 Objective of Present Research

This thesis focuses on using a pneumatic artificial muscle (PAM) in conjunction with several force sensitive resistors (FSRs) as the actuator system for a highly proprioceptive single DOF ankle exoskeleton. The system is designed to output forces useful for not only reducing, but amplifying the wearer's muscular exertion with forces in excess of 1g. This operation regime is unique to current, lower extremity exoskeleton developments, as it couples both speed and force, while using components suitable of a portable package. The use of FSRs in the context of closed loop control is also a novel development and will receive special focus. That being said, the first primary objectives of this research is (1) to design, fabricate, and test a PAM-based ankle exoskeleton prototype using components capable of controlled motion exceeding 3 Hz and exert ground forces exceeding 1g. The second primary objective is (2) to investigate and qualify force sensitive resistors as the input for a force control loop appropriate for exoskeletal use.

A strong emphasis was placed on a systems level approach including sensor selection and integration, as well as the actuator control chain. Additionally, the system was designed to be mechanically representative of a fielded device. This was done to unearth any non-obvious challenges and pitfalls of using PAMs for dynamic exoskeleton applications, and more realistically represent the performance of a PAM in this type of application. A commercialized version of such a system holds promise for military, medical, and industrial use. There has been interest expressed in increasing the

athleticism of American soldiers by efforts such as the Tactical Assault Light Operator Suit (TALOS) program [11]. Commercial devices of this nature could also present new use cases in the sports entertainment industry. One could imagine new entertainment activities or sports involving an exoskeleton that amplifies the wearer's physical prowess. In an industrial setting, offloading of tools supporting heavy loads could be done in a far more natural manner and more portably than current exoskeletons. It should be noted that any realistic commercial exoskeleton would require more than 1 DOF per leg. However, this study presents a generalized framework which could be largely applicable to subsequent DOFs proximal of the ankle.

1.3 Overview of Thesis

The majority of this thesis will focus on the concept development and design of the exoskeleton, as this effort did not inherit any substantial portion of a design from an existing exoskeleton. First, requirements development will be discussed followed by system level trades and decisions. Next, the design will be walked through in detail, focusing on the component level. Lastly, the integration and testing of the exoskeleton will be discussed, along with results and conclusions.

Exoskeleton Design and Fabrication

2.1 Requirements Development

Before designing the exoskeleton, specifications had to be derived to design a system capable of dynamic locomotion. For this application, tasks of running and jumping were selected as design goals for sizing components and selecting sensors. While running can involve impact forces in excess of 3g's, humans tend to exert closer to 2g's of equivalent force when running and jumping and producing net positive work [12], [13]. This exoskeleton, though it could be used to absorb impacts, is focused on producing net positive work for increased athleticism. For that reason a ground reaction of 2g's was targeted. The mass and dimensions of the designer and author were used for the sake of convenience and ease of testing. Weighing 75 kg, this resulted in a 2g force of 1470 N.

Rather than develop a complicated model to estimate a flowrate requirement to achieve dynamic motions, it was decided to select an oversized valve. This would result not only in adequate actuation speeds of the PAM, but also allow a faster control bandwidth due to the larger orifice size of the valve. Further details are discussed in the component design section.

Range of motion (ROM) is highly dependent on the action being performed as well as the physique of the wearer. Typical human ankle flexion range of motion can range from 59 to 79 degrees depending on gender and flexibility [14]. A typical walking gait only uses 25-40 degrees range of motion, running between 45 to 60 degrees range of motion [12], and jumping up to 70 degrees. For this research effort, it was decided to design mechanical hardstops at 60 degrees range of motion, offset for typical plantar vs.

dorsi-flexion limits, largely for safety. The PAM length would be maximized to allow as large of a range of motion as possible. Considering the significant force drop-off associated with PAMs throughout their stroke, even a ROM exceeding the hardstop ROM would still be advantageous, as more force would be available throughout the stroke.

The controller levied the requirement for a toe force sensor as well as a PAM force sensor and is discussed in detail in a subsequent section. Additionally, it was decided to require an ankle encoder even though not currently in the simplified control loop. This thesis focuses on the power stroke of the stride, which only involves force control. An encoder would be required for a controller managing a full running gait. These requirements are summarized in Table 2.1.

Table 2.1 System Requirements vs. Final Capability

Parameter	Requirement	Capability
Peak Ground Force	2g's (1500 N)	3.3 g's*
System Flowrate	Oversize	1300 slpm
Range of motion	60°	60°
PAM Force Sensor	Yes	Yes
Toe Force Sensor	Yes	Yes
Ankle Angle Sensor	Yes	Yes

*Theoretical max PAM force, not tested to this limit

2.2 System Level Controller Design

In order to allow highly dynamic, natural motions, a closed-loop force control scheme was decided on rather than a typical quasi-open loop architecture seen in other current semi-passive and active ankle exoskeletons [4]. This control architecture, though

more responsive to the wearer’s motions, requires that toe force be sensed in real-time. A block diagram of this control scheme can be seen in Figure 1.

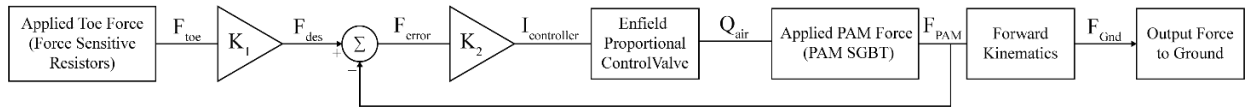


Figure 1. Force Control Diagram

Where F_{toe} is the force the wearer exerts with his or her toe, F_{des} is the desired force for the PAM to exert, F_{error} is the error between the desired PAM force and the actual PAM force, $I_{controller}$ is the drive current sent to the valve to displace the spool, Q_{air} is the flowrate of air into or out of the PAM, F_{PAM} is the retraction force of the PAM, and F_{Gnd} is the force exerted on the ground by the exoskeleton. In this control scheme, the force applied at the wearer’s toe is multiplied by gain K_1 , which can be thought of as an ‘assist ratio’. For example, for a K_1 value of 10, the PAM would nominally exert a force ten times more than the wearer is already pushing with. In a future version, there would be a forward kinematics calculation after the K_1 gain. For the simplicity, this was left out as it did not affect testing and results, given that K_1 is already arbitrary. This desired force is then sent to a feedback loop, where K_2 is a traditional proportional term used to track the changing F_{des} force trajectory. This output commands the valve, which adjusts the flowrate to and from the PAM by shifting the spool of the pneumatic valve back and forth. As compressed air is released into the PAM, a pressure is developed, which results in the PAM either displacing or increasing its force.

2.3 Mechanical Design

2.3.1 System Level Mechanical Overview

A simple lever arm kinematic structure shown in Figure 3 was decided on. This is the most common structural and kinematic configuration of existing ankle exoskeletons. It requires a tensile actuator, which is appropriate for a pneumatic artificial muscle. This configuration provides robustness, as well as structural stiffness to allow high bandwidth control schemes. In the architecture shown, a PAM exerts a tensile force on an armature. This creates a torque about the ankle, which is reacted against the ground through a passive toe joint. A CAD rendering of the final design can be seen in Figure 2, after which all the major components of the exoskeleton will be walked through individually.

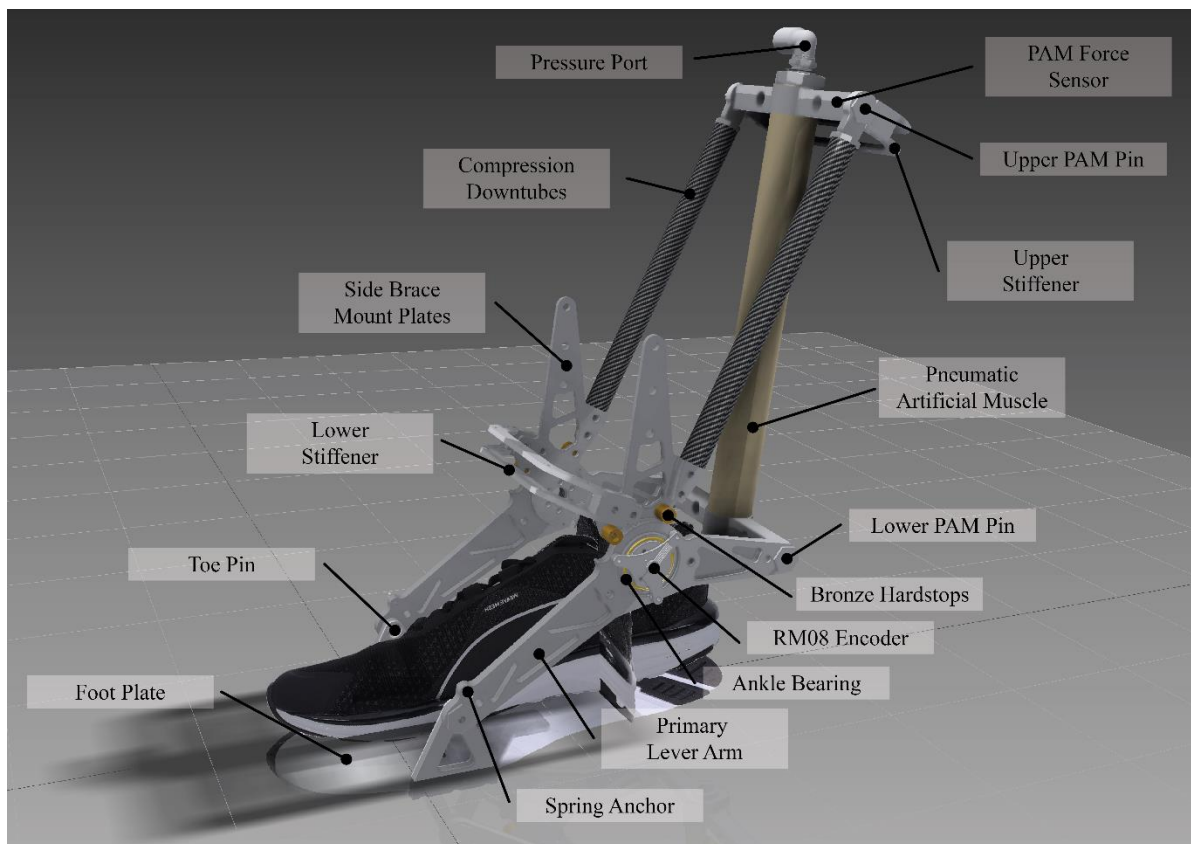


Figure 2. CAD Rendering of Ankle Exoskeleton

2.3.2 Actuation Technology Trade

Pneumatic vs. Electric

Pneumatic Artificial Muscles (PAMs) exhibit high force and power outputs relative to their comparatively low mass and volume. The most common type of actuator, electric motors, require a gearbox to reach forces and torques at the level of walking and running, whereas PAMs output much higher forces with no force amplification, and move at a useful speed. Because motor rotor inertia gets multiplied by the gear ratio squared, the a typical ratio of 100:1 – if not more – results in an output inertia 10,000 times higher at the output than the rotor itself. Gearboxes also exhibit low efficiency and backlash, making them hard to backdrive and nonlinear when switching directions.

In contrast, PAMs have very low mechanical impedance, making them well suited towards exoskeleton applications where it is desirable for the wearer to experience minimal drivetrain inertia or drag. The challenge of making an exoskeleton feel as though it is not being worn yet still produce net useful work (i.e. energy) has been one of the hardest challenges in the field. Due to their high stiffness, the time constant with which electric motors must react for the wearer to feel no noticeable resistance is extremely short. Schemes must be adopted to predict the gait of the wearer, which does not allow for dynamic, unpredictable motions. PAMs are a lot more promising for this challenge, as they have multiple magnitudes less inertia compared to the output of an electric motor. They can accelerate, change direction, and be backdriven much easier and with less hysteresis than electric motors.

Lastly, motors are always designed to balance both speed and torque by choosing an appropriate gearbox and winding configuration for the task at hand. In other words,

motors are power limited, and there is a linear relationship between motor mass and power output. Having a bigger battery does not mean the motor can torque harder or spin faster, as this would cause the stator coils to either overheat (if current is too high) or experience dielectric breakdown (if voltage is too high). In the case of pneumatic (and hydraulic) systems, however, actuators are primarily designed to meet a target force. Actuator speeds are driven largely by the control valve, and it is much easier to reach very high speeds by simply picking a valve with a larger orifice. Additionally, pneumatic and hydraulic systems can direct full airflow or pump flow to a single actuator, whereas electric systems must make each individual actuator large enough to handle peak power draw.

Pneumatic vs. Hydraulic

Compared to the next most common actuation technology – hydraulics – PAMs are lighter and more energy efficient from a systems perspective. They are also far more compliant, which makes them safer to use, but harder to control. Hydraulics exhibit higher force output than PAMs for the same *volume* because working pressures are higher, and also have a linear force output across their stroke assuming the most common type of hydraulic actuator, a single-rod dual-acting cylinder. However, due to the large amounts of metal – typically steel – and liquid working fluid hydraulics exhibit lower force per unit *mass* than PAMs, which are typically made of a Kevlar or plastic overbraid, elastomer, aluminum, and use compressed air as the working fluid. Additionally, the required power packs for hydraulics are complex and heavy, making them ill-suited to mobile applications such as exoskeletons. In the context of robotics, hydraulics excel in position control applications due to the high modulus of the working

fluid. However, this high modulus works against them in the force control regime. Like electric motors, small displacements can quickly cause forces to spike, and the sensor and control system must be extremely fast to create an effective, low impedance system. The combination of these factors led to deciding against hydraulics as the actuation technology for a high power, dynamic ankle exoskeleton.

Pneumatic vs. Minority Actuation Technologies

Though electric, pneumatic, and hydraulic actuators encompass nearly all actuators, a number of less-used alternative actuation technologies exist. Some are many decades old and others more recent. Some of these alternative actuation technologies include shape memory alloys (SMA), magnetorestrictive alloys (MRA), piezoelectric actuators, voice coils/solenoids, controlled chemical reactions, artificial muscles, and electro-osmosis to name a few. However, none of these actuation technologies exhibit anywhere near the power density and controllability required to be a viable contender for an exoskeletal actuation technology.

Pneumatic PAM vs. Pneumatic Cylinder vs. Pneumatic Rotary Vane Actuator

Even once pneumatics was decided on, the type of pneumatic actuator still had to be traded. The three feasible types of pneumatic actuators were PAMs, cylinders, and rotary vane actuators. The overwhelming factor to pick PAMs is their high force density compared to similar size or mass cylinders and rotary vane actuators. PAMs take advantage of the overbraid structure to exhibit much larger forces than pneumatic cylinders of the same outer diameter. Also, cylinders and vane actuators are made nearly entirely of metal and therefore weigh much more than PAMs. The one advantage of using cylinders or vane actuators is their flat force or torque output across their stroke. This was

outweighed by the previous factors in favor of PAMs. As mentioned earlier, the natural walking, running, and jumping force profiles tend to decrease towards full ankle extension anyway, so a flat force profile isn't as advantageous given the application.

2.3.3 PAM Design

As described in the previous section, a ground reaction force of 1470 N is desired to perform dynamic motions. The force required by the PAM to exert this force can be calculated using the kinematic equations of the system. Though PAM design is discussed prior to structural design within this thesis, in practice both the PAM and structure were designed in parallel. Structural design will be discussed next in Section 2.3.4.

As shown in equations 1 through 3, a PAM force of 2225 N is required at push-off to achieve a 2g force. Recall that a wearer mass of 75 kg was used for sizing.

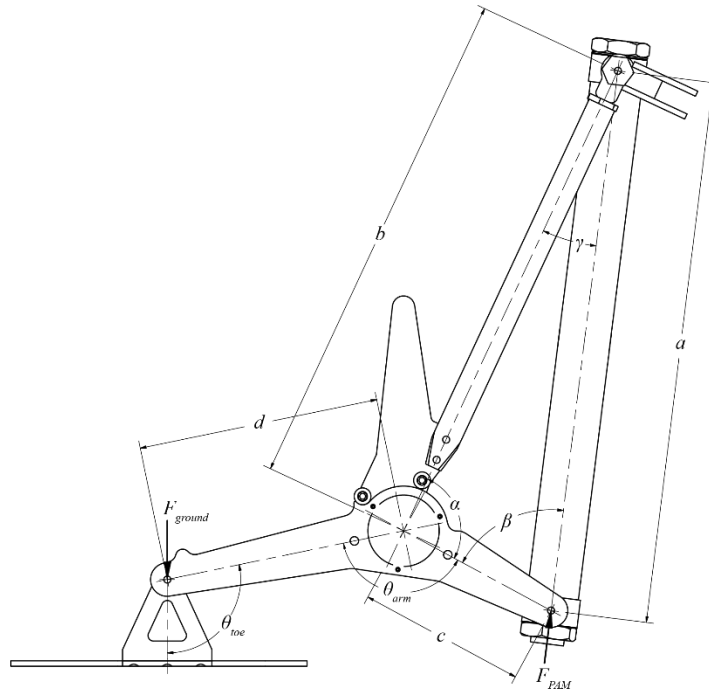


Figure 3. Side View of Ankle Exoskeleton

$$F_{ground,des} = 2 * m * g = 1470 N \quad (2)$$

$$\tau_{ankle,des} = F_{PAM} * c * \sin(\beta) = F_{ground} * d * \sin(\theta_{toe}) = 191 Nm \quad (3)$$

$$F_{PAM,des} = \frac{F_{ground} * d * \sin(\theta_{toe})}{c * \sin(\beta)} = 2225 N \quad (4)$$

Though this force can be achieved with a reasonably sized PAM of less than 1” diameter, PAMs exhibit a highly nonlinear force vs. stroke profile and the load drops off quickly as a function of stroke. For this reason, it was decided to target the 2g force at the beginning of the stroke, but not throughout the entire stroke. This is also representative of a typical human jump, which reaches a peak force quickly, then continually drops to zero as the athlete leaves the ground. The PAM was designed so that at a reasonable max operating pressure of 6 bar (90 psi), the force would exceed 2g’s for the first third of stroke, 1g for the second third, and drop to 0g by the end of its stroke. The estimated curve is shown in Figure 4 using the PAM model from [15].

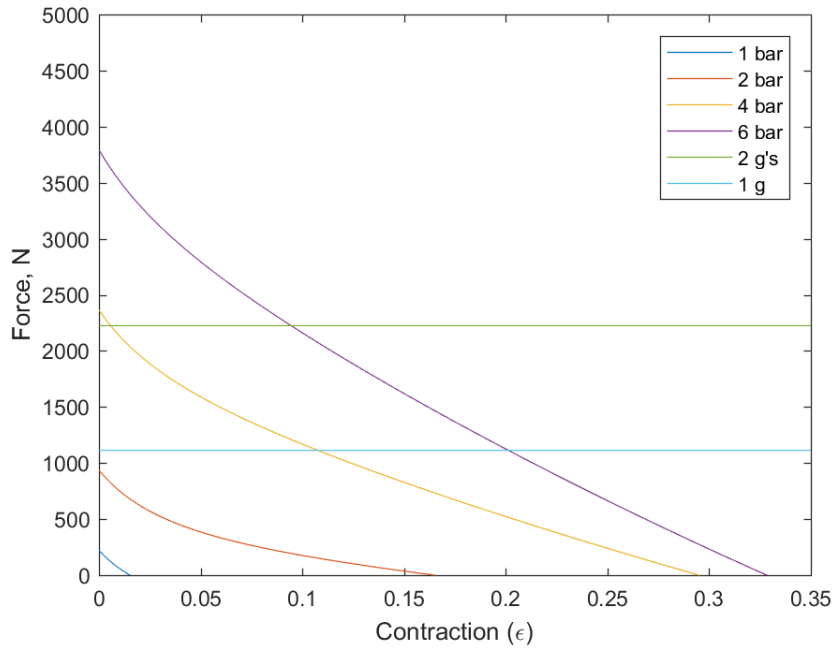


Figure 4. Theoretical PAM Force vs. Deflection vs. Pressure Curves

A block force of 3750 N was estimated, correlating to 3.3g's of force or 318 Nm torque about the ankle. Given a stroke of 32%, a range of motion (ROM) of 60 degrees could be achieved with 9.5 cm of stroke, correlating to a free length of 29.5 cm. Meeting this length requirement was very difficult, as the available room behind the calf muscle is not much longer than this to begin with.

The mechanical design of the PAM itself is based off a design from [16], which utilizes the wedge phenomenon to both seal and mechanically constrain the Kevlar braid using a conical 7° taper shown in Figure 5. Custom armatures are required to maximize stroke length and meet the range of motion requirement, making the pivot points of the PAM in-line with the end cap itself instead of taking up additional length. Both ends of the PAM are identical, except that one side uses a 3/8 inch push-to-connect fitting and the other an NPT plug.

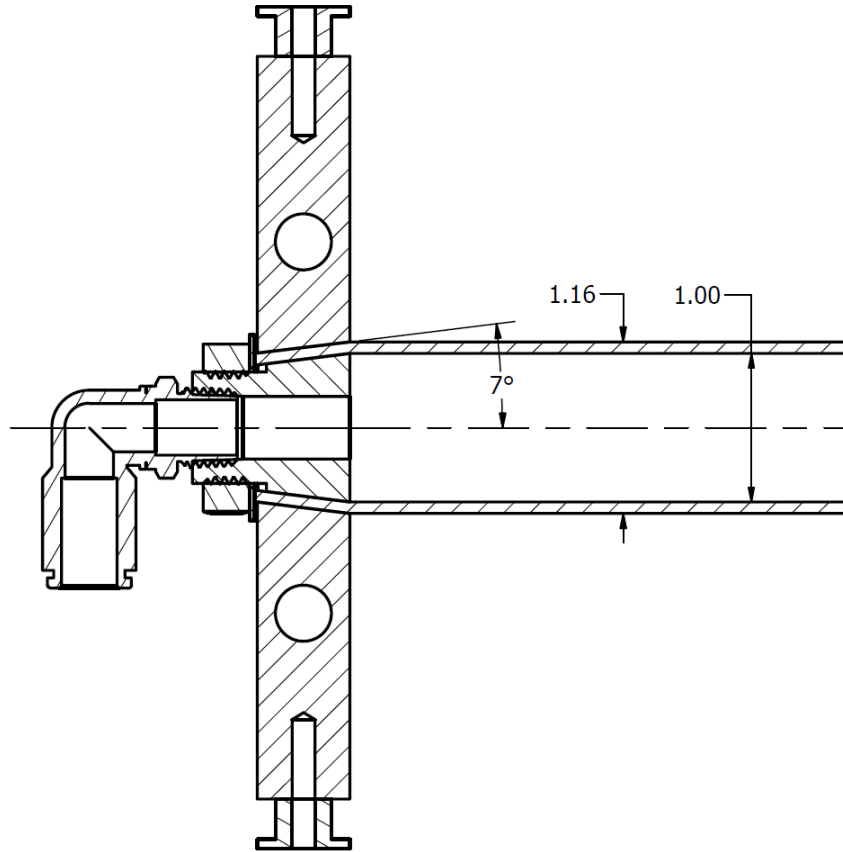


Figure 5. PAM Cross Section

The armatures of the PAM are also designed to accommodate a full-bridge strain sensor, used to output the force of the PAM in a compact manner, as a commercial load cell would have reduced stroke and thus ROM below the requirement. This sensor will be discussed further in the proprioception section.

Power source, fielded endurance estimate

For this design, it was decided to use an off-board pressure source for the sake of simplicity and scope. Though not the focus of this thesis, a brief energy study was performed. One of the most viable technologies to make the exoskeleton fully portable is paintball composite tanks, which store air at 310 bar, many times higher than the

exoskeleton working pressure of 7 bar. Assuming the braid is in a maximum contracted state and at the max braid diameter of 5cm we know volume of a cylinder is defined as

$$V = \frac{\pi d^2}{4} * L \quad (5)$$

where $d = 0.05\text{m}$ and $L =$ the contracted length of 0.20 m . Thus, the approximate volume of the contracted PAM is $3.93\text{E-}4\text{ m}^3$. Based off of the ideal gas law and assuming adiabatic expansion, we know

$$\frac{p_2}{p_1} = \left(\frac{V_1}{V_2}\right)^\gamma \quad (6)$$

where p_1 is the PAM operating pressure of 6.2 bar , V_1 is the equivalent volume of air available to be used by the PAM at its working pressure (the variable we will be solving for), p_2 is the paintball tank storage pressure of 310 bar , and V_2 is a typical paintball storage capacity of $1.44\text{E-}3\text{ m}^3$, and γ is 1.400 , the unitless heat capacity ratio of air at 20° C . Solving for V_1 yields 0.0235 m^3 , or 60 times greater volume than the PAM at its own working pressure. This would be equivalent to only 60 steps at max force and extension.

To try and achieve a more useful energy number and upper estimate on endurance, it is assumed that two compressed air tanks can be worn, which is reasonable at only 370 grams each for a typical 88ci ($1.44\text{E-}3\text{ m}^3$) composite tank. It is also assumed that only half the working pressure is used (on average), and isothermal expansion instead of adiabatic, which is defined by the equation

$$\frac{p_2}{p_1} = \frac{V_1}{V_2} \quad (7)$$

This yields a volume of 0.288 m^3 or 733 times more than the volume of the PAM. Assuming a stride frequency of 2 Hz , these two calculations would yield endurances of

0.5 minutes and 6.1 minutes respectively. Neither case is especially long or useful for anything besides the sports and entertainment industry. If a duty cycle of 25% were assumed due to standing still, running at a slower stride frequency, etc, the latter case would yield a 24 minute run-time, which is beginning to enter the realm of usefulness. Ultimately, field testing would be used to the longevity of the device. Though these results may be alarming, it is to be expected as highly dynamic motions are far more taxing from an energy standpoint than most systems that currently exist.

2.3.4 Exoskeleton Structural Design

The exoskeleton structure consists of several dozen custom and COTS parts. They will be discussed individually, starting at the PAM anchor points and following the load path through into the ground. This will provide an intuitive understanding of the exoskeleton functionality, as well as how each component was designed.

PAM Interface

It was decided locate the PAM along the center plane of the exoskeleton, resulting in zero net moment about the roll axis (i.e. forwards pointing, sagittal axis). This allowed for much lighter, single-load optimized structural elements while maintaining high stiffness. Were the PAM to be located on the side of the exoskeleton, it would require the structure to react high roll moments, which would be especially hard at the targeted forces. A downside of having a centered PAM, however, is that there is a minimum lever arm length between the ankle and the load application point of the PAM as well as a maximum PAM length limited by the height of the thigh when in a lunging position. This

made meeting a 60° requirement one of the hardest requirements, but kept down the exoskeleton mass.

The PAM is anchored into two PTFE-lined TIN-bronze bushings, press fit into an aluminum waterjet-cut piece. Teflon lined bushings were selected for their high load capacity in conjunction with low friction without any lubrication required. A commercial McMaster part was used: P/N 60695K2. The bushing was cut in half to minimize the width of the exoskeleton and allow use of quarter-inch aluminum stock for easy waterjet manufacturing. The load capacity of a single bushing was already four times greater than the expected max PAM load, and only reacts approximately half the load due to geometry, so this modification was acceptable. Two waterjet pieces are sandwiched with aluminum spacers in between them to act as a lateral stiffener between the two sides of the leg. These parts add a great level of stability to the structure, forcing the two sides to move in unison with each other. Because they are minimally stressed and already very lightweight, no structural analysis was performed on them.

Carbon fiber rods and rod replacements

The PAM load gets reacted from the bushing into a carbon fiber rod intended for compression. When the free body diagram was drawn to estimate the load on the carbon fiber rod, it was incorrectly derived that the rods only experienced compression as the PAM was contracted. However, it was discovered after construction that they experience both compression as well as a bending moment. They were not rated for the high bending moment the full PAM would produce, and therefore, the PAM pressure was limited to 1.5 bar, roughly one fifth of its intended working pressure. Though this is a severe design flaw, the testing was still carried out and the results proved to be insightful and useful.

Though not fabricated, an alternate structural element was designed. A finite element analysis (FEA) model was created to analyze the stresses in all structural parts. These results are shown in Figure 6.

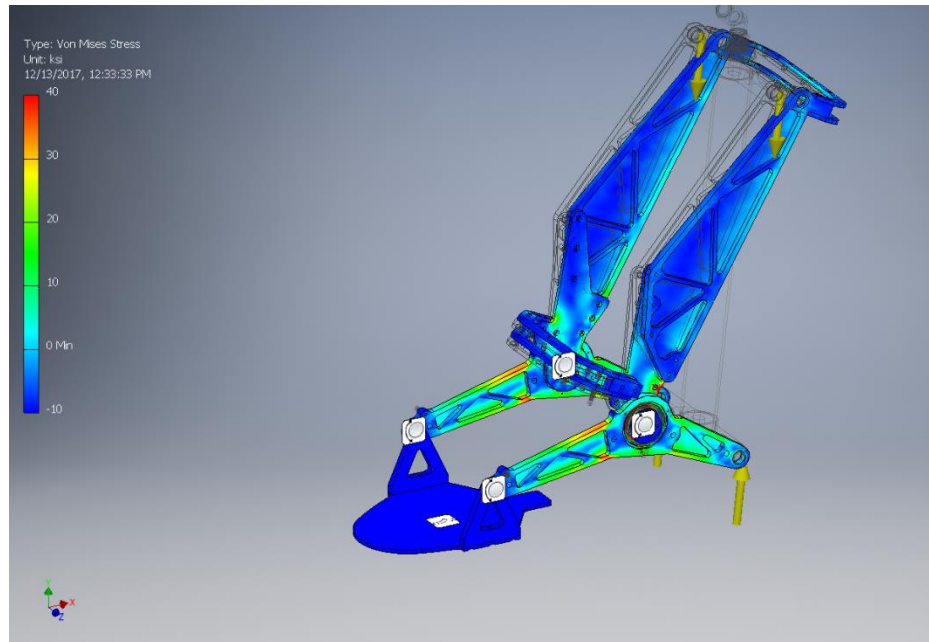


Figure 6. FEA results

Looking at the FEA results, the newly designed structural element is able to handle the bending moment with maximum stresses rarely exceeding 70 MPa, compared to the AL 6061-T6 yield strength of 240 MPa.

Side interface plates

Load from carbon fiber downtubes is reacted into two 3.2mm thick waterjet cut aluminum plates referred to as “side plates”. The side plates interface with a number of elements including the downtubes, the ankle brace, a lower stiffener, bronze hardstops for both extension and flexion, as well as the ankle shaft. Like the carbon fiber downtubes, this part was intended to react only compression coming down the carbon fiber tube, not bending. However, performing the analysis and including bending stresses, the yield

strength of the material is only exceeded in one area due to a small stress concentration. A small amount of local yielding would be expected to occur, after which the part would be able to withstand the full applied loads.

A second stiffener was added to maintain symmetry between the two sides of the exoskeleton. As shown in Figure 7, the hardstops mounted to this part are made out of bronze to absorb impacts with less shock than a steel part. They constrain the range of motion to safe limits for the wearer.



Figure 7. Bronze Hardstop

The ankle shaft shown in Figure 14 interfaces to the side plate through a six-hole bolt pattern, which reacts the load of the PAM through shear. A set screw was modified to embed a 4mm cylindrical in it, letting the ankle angle to be measured by the RM08 encoder from Renishaw.

Ankle Brace

The actual interface to the wearer is a commercial ankle brace designed to ergonomically fit around the wearer's lower leg. A Shock Doctor V-Flex Ankle XT Brace was selected because it had a number of plastic elements which could be modified to bolt into the exoskeleton frame. The exoskeleton was bolted through in six places,

sandwiched by large surface area plates to distribute the load evenly into the plastic structure and into the wearer's leg.

Ankle Bearings

Load from the PAM is reacted through the ankle shafts into two flanged thin-section deep-groove radial ball bearings, type F6805ZZ. With a load rating of 4300 N each, these bearings can handle the max PAM load of 3700 N divided roughly equally between the two of them. In instances where the wearer is leaning heavily to one side (i.e. leaning sideways while cutting), the assumption of equal loading would not apply. This load scenario was ignored for this prototype.

Lever Arm Plates

Load is passed through the ankle bearings into two lever arm plates, which are the primary kinematic element in the exoskeleton. These components rotate about the ankle axis, reversing the PAM direction of applied load into the ground to create a vertical accelerating force. Like the side interface plates, there were several stress concentrations that exceeded the 240 MPa yield stress of the part (e.g. fillets in lightweighting pockets). However, the gross structure is able to handle the full torque applied about ankle exoskeleton with margin on yield strength. The second PAM anchor points are located on the posterior side of the lever arm plates. The same PTFE lined bushings are used here as at the top of the carbon fiber downtubes. The anterior side of the lever arm plates interfaces with the toe plate.

Toe/Ground Plate

It was decided to add a passive joint at the toe to allow for greater agility, as the bending of the toe is critical to both running and jumping. The load transmitted through

the lever arm plate is reacted through another PTFE lined bushing into two triangular aluminum waterjet cut pieces, each a quarter of an inch (6.4mm) thick. These components are fastened to a ground plate, where the load is finally reacted into the ground. There are three force-sensitive resistors taped to the top of this ground tape using ~1mm thick foam double sided tape. The tape adds a small amount of compliance and load distribution to the FSRs, which prevents pressure concentrations caused by imperfections in the aluminum plate. The sole of the shoe provides adequate compliance from the top side, to prevent pressure concentrations that would cause a non-linear response between applied force and the FSR electrical signal. These sensors will be discussed more in subsequent sections.

2.4 Electrical, Proprioception Design

2.4.1 System Level Electrical Overview

There are three sensors on the exoskeleton: a sensor between the toe and the ground plate to sense applied force, a sensor measuring the PAM force, and an encoder on the ankle joint. There is also a fourth sensor used only for testing – a weight plate to measure ground contact forces. These sensors interface to a central microcontroller, which performs all input/output (I/O), as well as handles the controls algorithms. There are only two external components to the exoskeleton: an off-board compressed air source and a PC, which accepts a serial data stream to capture data for testing. The microcontroller selected was an Arduino Due. One of the newest generations of the Arduino, the Due most notably is controlled by a 32 bit processor, capable of performing far more complex algorithms than its predecessors. In the case of the exoskeleton, this allowed control loop speeds in excess of 1000 Hz.

Figure 8 shows an overview of the I/O components, which will be described in further detail in the component level design section.

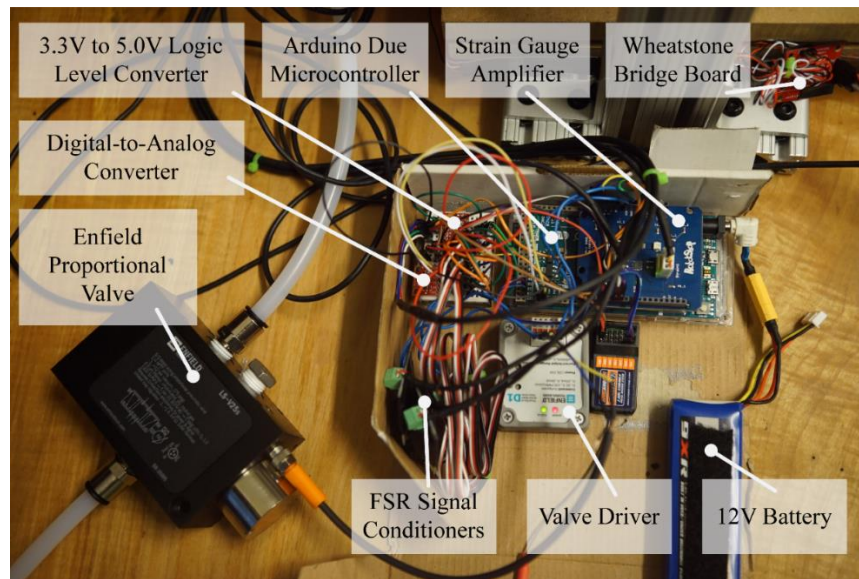


Figure 8. Control Electronics

All the electronics were packaged into a thigh pouch that could easily be worn by the user. The as-built exoskeleton along with the electronics are shown in Figure 9.



Figure 9. Exoskeleton and packaged electronics

2.4.2 Actuator Control Scheme

In order to allow precise control of the PAM at high speeds, a proportional valve was required. The Enfield LS-V25s [17] is capable of high bandwidth control at high flowrates, and is more affordable than the only other notable proportional valve manufacturer (Festo Corporation). It requires a ± 1 amp signal to control it, which the corresponding Enfield D1 driver supplies. The D1 driver is controlled via a 0-5V analog signal. The Arduino sends this signal using a 5V DAC connected via I2C. This control scheme is shown in Figure 10. Initially a direct DAC line on the Due was used. However, this signal had a full scale output (FSO) of only 3.3V, which limited the PAM velocity in the return stroke.



Figure 10. PAM Control Chain

2.4.3 Proprioception Development

As mentioned earlier, a large focus of this research effort was to focus on relevant proprioceptive technologies and their implementation in realistically packaged ankle exoskeleton application. This section investigates the use of several proprioceptive technologies used in tandem with the PAM to naturally amplify the wearer's motions in a fluid manner. These sensors consist of a matrix of thin film force sensitive resistors, a custom strain gauge based transducer integrated into the PAM structure, and a commercial-off-the-shelf (COTS) angular encoder about the ankle axis. A weight plate is also developed to assist verifying the output of these sensors.

Applied Toe Force Sensor

The force exerted by the toe is a valuable control input not typically seen in ankle exoskeletons, as it is very hard to implement. It is desirable for the foot to be very close to the ground, leaving no room for a sensor. Furthermore, the centroid of applied load is constantly changing as the user shifts weight. For these reasons, commercial strain gauge based load cells are not appropriate for this application. Instead, force sensitive resistors (FSRs) were selected for this application. Though they do not exhibit the repeatability or linearity of a commercial load cell, they are one of the only sensors that fit within the desired package constraints. FSRs don't measure force directly, but respond to applied pressure, meaning a single large FSR cannot be used to estimate toe applied force. This is because a low force applied over a small area would give the same reading as a large force applied over a large area. In a realistic end use application, a matrix of several dozen small sensors would cover the area of the foot, with pressure readings numerically integrated to estimate applied force. There are several emerging companies selling this technology on a limited basis for applications such as measuring power output when running. A pair of these insoles was ordered from the French company, Feetme [18], with the intent of reverse engineering and implementing into the exoskeleton. However, the product was brand new and was not received during this research effort. Instead, three 25 mm diameter FlexiForce force sensitive resistors were used, acquired from Sparkfun [19], as well as signal conditioners from Robotshop [20] to linearize the signal. Because the sole of a shoe naturally exhibits some level of load spreading, this helped prevent sharp load concentrations which would cause false load outputs. For an end-use application, more sensors would be added for better coverage and more robust feedback.

Additionally, it could be advantageous to locate the sensors within an insole of the shoe rather than underneath it. A shoe with an aggressive pattern could cause erroneous readings depending on its durometer and pattern.

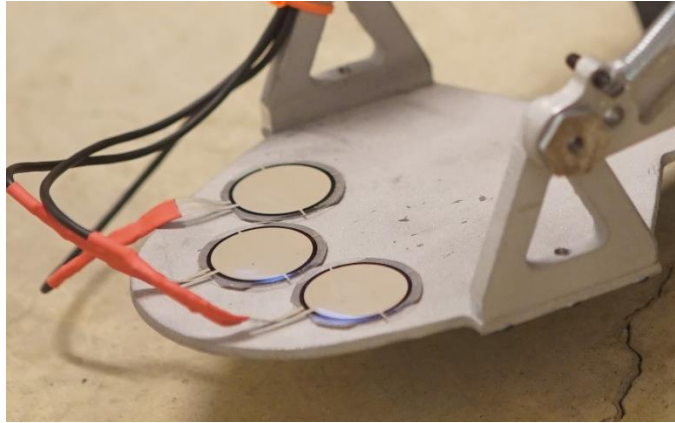


Figure 11. Commercial FlexiForce Sensors Integrated on Toe Plate

PAM Force Sensor

A strain gauge based transducer (SGBT) was developed to measure PAM force. The sensor was designed to measure axial PAM loads up to 5000N. Strain is controlled by adjusting the diameter of two through holes in the armature of the PAM. These hole sizes adjust the moment of inertia of the armature cross section, and therefore strain profile of the section, allowing the strain at the surface to be controlled. The profile of the spring element is shown in Figure 12.

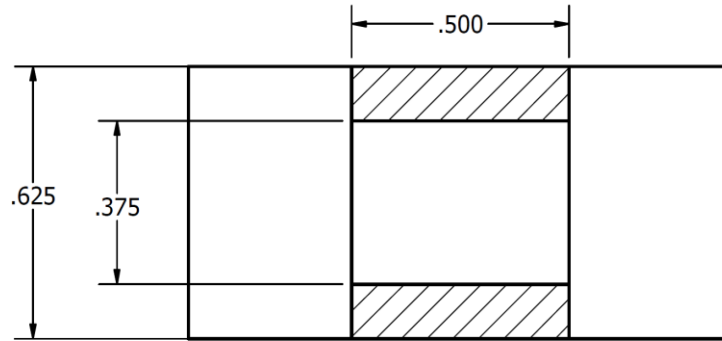


Figure 12. PAM SGBT Spring Element Cross Section (units are in inches)

The inertia of the cross section about its central axis can be calculated from the equation for an offset rectangular section

$$I_{xx} = \frac{b \cdot h^3}{12} + a \cdot d^2 \quad (8)$$

Where I_{xx} is the area moment of inertia of the cross section, b is the base width of 12.7 mm, h is the rectangular height of 3.18 mm, a is the rectangle area of 40.3 mm², and d is the offset of the centroid from the axis the inertia is being calculated about, 6.35mm in this case. This yielded a total moment of inertia of 1658 mm⁴. The maximum stress can be calculated from the corresponding equation for stress along a cross section under bending

$$\sigma_{max} = \frac{M \cdot y}{I} \quad (9)$$

where σ_{max} is the max stress and M is the applied moment at FSO, given by $F \cdot r$, where F is 1875 N (max load divided in half) and r is 31.8mm given geometry. This assumes the bushing cannot support a lateral moment, creating fixed-free configuration. y is the location of max stress, or the outermost point on the section at 7.94mm, and I is the moment of inertia calculated above. This yields a maximum stress of 143 MPa. Using the modulus of the material, we know

$$E = \frac{\sigma}{\epsilon} \quad (10)$$

where E is the modulus of aluminum, 68.9 GPa, σ is the stress calculated above, and ε is the strain being calculated. Solving for ε yields 2071 microstrain. Though transducer grade SGBT's typically target a strain of 1500 microstrain [21], going slightly higher than this is acceptable for an R&D effort, and also provides a higher signal-to-noise ratio, increasing resolution. For this effort, providing good sensory data is more valuable than maximizing life and overload protection of components.

The sensor itself utilizes two half bridge tee-rosette strain gauges from Micro Measurements to create a full wheatstone bridge. This configuration helped reject thermal drift as well and off-axis loading, and optimize the milliamp-level signal for better signal-to-noise ratio. A Robotshop 2-channel wheatstone bridge amplifier was used to amplify these signals for input into the microcontroller. The gauges were installed using Micro Measurements instruction manual B-130, consisting of a 4 hour cure at 130°C followed by an elevated, unclamped post-cure at 165°C prior to soldering the leadwires on and coating with environmental protection. The components used to fabricate this transducer as well as a picture of the final transducer are shown in Table 2 and Figure 13 respectively.

Table 2. Components Used for Strain Gauge Transducer Fabrication

Component	Vendor	Quantity (per sensor)	P/N
Strain Gauge Foil	Micro Measurements	2	N2A-06-S150R-1KB
Bondable Terminal	Micro Measurements	1	CPF-50C
Bonding Adhesive	Micro Measurements	-	M-Bond 610
Environmental protection coating	Micro Measurements	-	M-Coat A
Intrabridge wire	Micro Measurements	<1m	134-AWP
Shielded leadwire	Mogami	~1m	2929-00
Amplifier	Robotshop	1	RB-Onl-38



Figure 13. Assembled PAM SGBT

Ankle Encoder

A COTS absolute magnetic encoder was used to sense the ankle angle. As one of the smallest commercially available absolute sensors in the world with a 12-bit signal, the RM08 packaged efficiently and eliminated the need for a calibration routine on startup. It is also non-contact, utilizing a 4mm cylindrical magnet bonded into the ankle shaft to acquire the rotational position. Because the microcontroller operates at 3.3V and the

RM08 at 5V, a 3.3-5V logic level converter was used for the SPI communications between the RM08 and the Arduino Due. The sensor and actuator (magnet) are shown in a disassembled state in Figure 14.

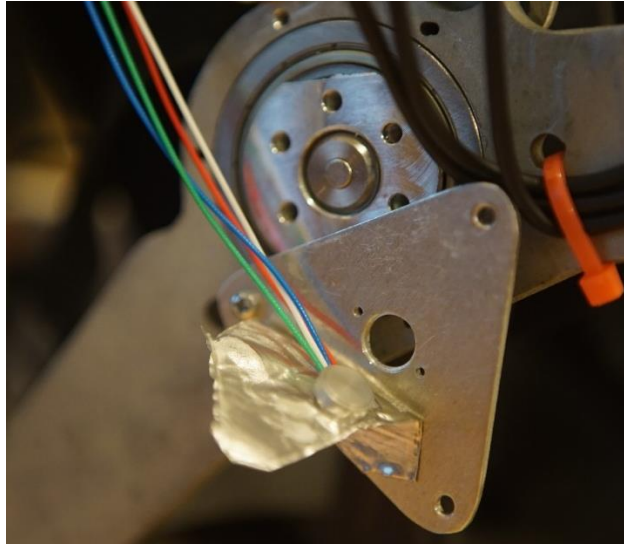


Figure 14. RM08 Encoder and Shaft Magnet

Weight Plate

Lastly, a weight plate was designed and fabricated for testing purposes, to calibrate all the sensors. The weight plate consisted of four quarter bridge button-type load cells [22] rated to 50kg each, located at each corner. Because the load cells support the applied load in parallel, the capacity is 200 kg, or 2.6g's for the design mass of 75kg. Due to the nature of the wheatstone bridge, the output of the bridge is insensitive to the location of the applied load, so long as it is applied within the perimeter of the four load cells. This technology is similar to that used in typical digital bathroom scales, except the signal conditioning and data acquisition is capable of high bandwidth for control and testing purposes. The plate itself was machined out of medium density fiberboard (MDF), with pockets and features added to positively seat and locate the button load cells. This

allowed the fixture to react a shear load without the upper board sliding. The weight plate is shown in Figure 15.



Figure 15. Weight plate showing button load cells (Left) and upper plate installed (Right)

Sensor Qualification and Characterization

All custom sensors used needed to be qualified experimentally. This section outlines the process of characterizing and qualifying these sensors for use.

3.1 Weight Plate Qualification

The weight plate was straightforward to qualify. Due to the robustness of the sensors, a linear load versus voltage relationship was assumed. The sensor output was tared and a 160lb weight applied (user standing on the plate) to determine the scaling factor. This weight plate was used in subsequent tests to verify and calibrate the toe sensors as well as PAM force sensor. The value of the weight plate is retrieved in the same manner as the PAM force sensor, which is described shortly.

3.2 Toe Force Sensor Qualification

To qualify the toe contact force sensors, the weight plate was used. Load was applied to each of the force sensitive resistors (FSRs) and the output plotted versus the weight plate load (the control). The outputs of these tests gave linearity curves for the three sensors and is shown in Figure 16.

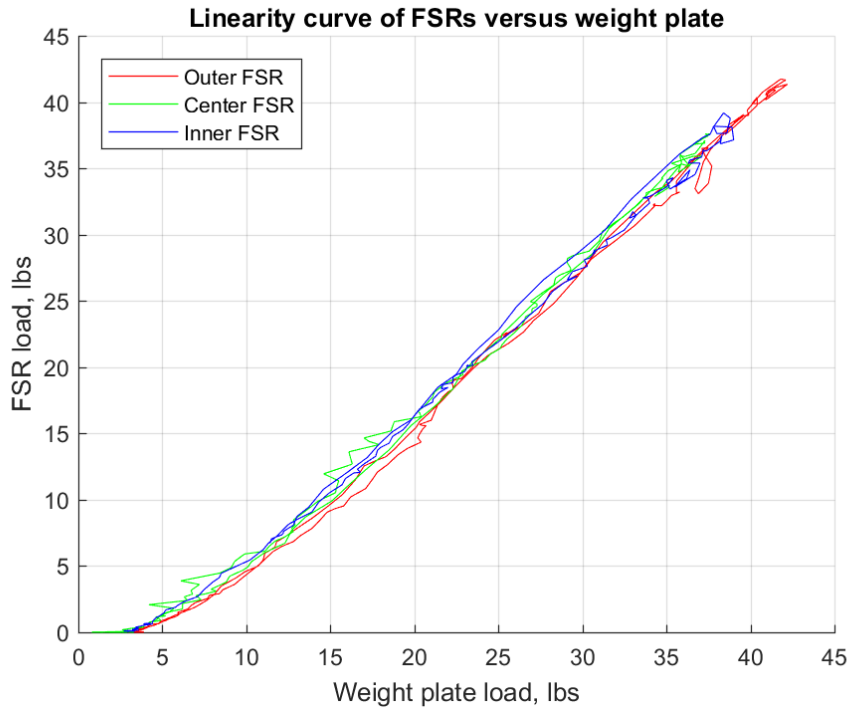


Figure 16. FSR output force versus actual load

As seen in Figure 16, these sensors have observable error, but are still likely adequate for the task at hand. More notably, they exhibit extremely low hysteresis, which is far more important for an exoskeleton application than linearity. Consider typical biological sensory systems. A human does not exert and exact force (e.g. 26.3N), but rather responds gracefully to resistances and disturbances based off of proprioceptive feedback. Likewise, FSRs are only moderately accurate, but are highly responsive and can sense small directional deviations important for closed loop control.

Next, the sensors were tested in tandem with each other by wearing the exoskeleton with all three installed. The sensors were subject to several different loading scenarios while standing on the weight plate, as depicted in Figure 17.



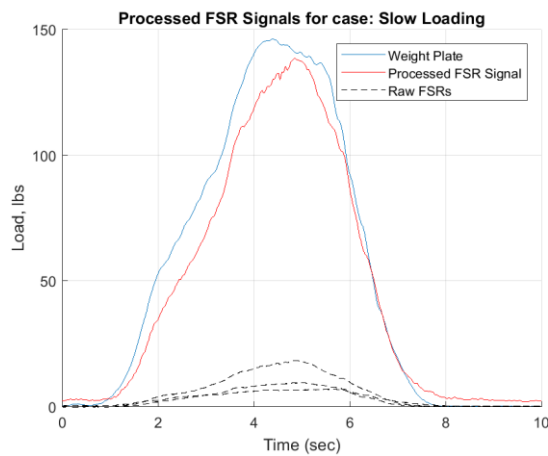
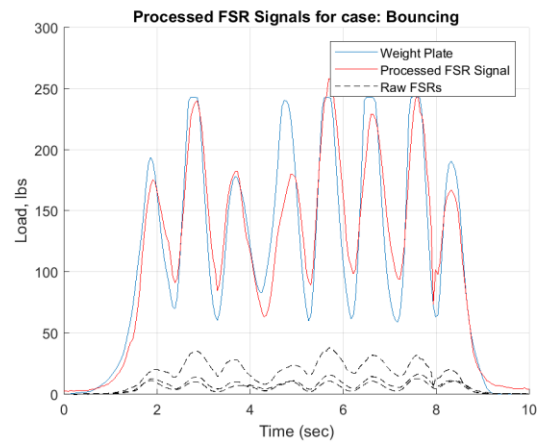
Figure 17. Testing FSRs integrated onto exoskeleton

Because the sensors do not entirely cover the ground plate, the sum of applied load is only a portion of the actual toe force. Several algorithms were tested to estimate the actual applied ground force from the three sensor signals. In the end, the average of the three signals was taken, and multiplied by a constant scaling factor which was empirically determined.

$$F_{GND} = \frac{K_{FSR} * (F_{FSR,1} + F_{FSR,2} + F_{FSR,3})}{3} \quad (11)$$

These results are shown in Figure 18. The images below all used the same constants, and exhibited seemingly adequate accuracy and dynamic response, though not the fidelity of a commercial SGBT. The largest source of error is most likely the fact that not all the load goes through the FSRs, because they do not fully cover the contact area between the shoe and the ground plate. The model used assumes a linear relationship between applied force and combined sensor output. However, when the wearer shifts weight anterior or posterior, the sensed vs. unsensed weight distribution is non-linear.

The sensors are more robust towards left/right weight shift than anterior/posterior weight shift because they are situated roughly in line with each other along the sagittal plane. As mentioned previously, this could be largely compensated for by using a large number of small sensors covering the entire ground plate or even foot area. This was not feasible given the scope and resources of this thesis, but would be reasonable for a commercial product. This thesis is more focused on their use in a closed loop controller, which will indicate their suitability as a high bandwidth trajectory control sensor.



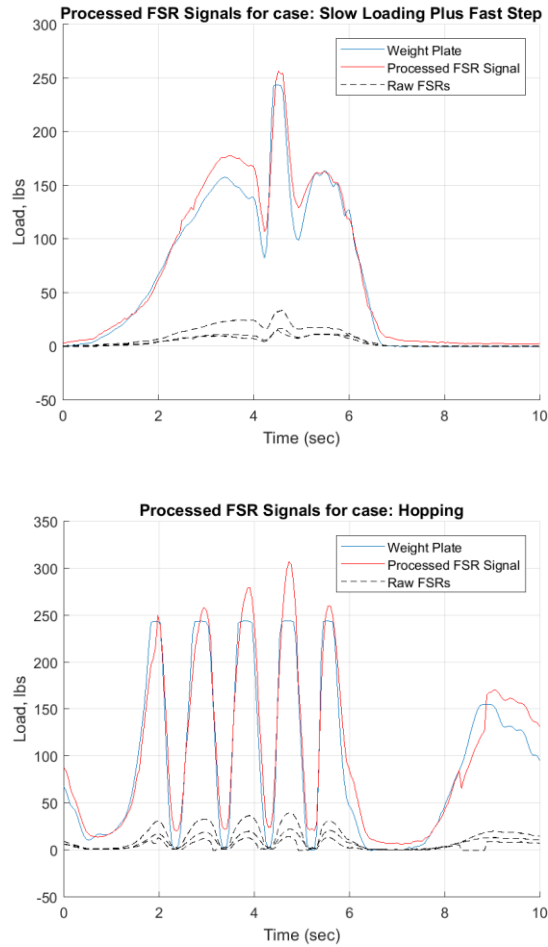


Figure 18. Processed FSR signals versus weight plate signal

3.2.1 PAM Force Sensor Calibration

Because the interface to the PAM was specifically designed for the exoskeleton, it was not straightforward to apply a load in a benchtop setting. Rather, the PAM was actuated and the weight plate load noted. The theoretical load on the PAM was estimated using the kinematics of the structure, assuming friction to be zero. Though the scaling factor could have been achieved in a more accurate manner, the focus of this paper is to investigate the performance of various sensors in tandem with each other, not quantify

the parameters of said sensors with high fidelity. The zero point and dynamic response of this sensor is important, but knowing its scaling factor with high accuracy is not.

Because the PAM SGBT uses standard strain gauges, common spring element material (6061 Aluminum), and the max stress is within the yield of the material, the response is assumed to be highly linear. As mentioned previously its signal is amplified using Robotshop Amplifier RB-Onl-38. Its force is retrieved by calling the `analogRead(A1)` function of the arduino. It is important to note that on the Arduino Due, analog voltages can be read at 12 bits instead of 10 bits, like its predecessors. This higher resolution is expected to have given a noticeable increase in smooth response.

3.2.2 Ankle Encoder Calibration

The RM08 relies on a 4mm cylindrical magnet embedded in the ankle shaft to encode its position. The distance between this magnet and the readhead is specified in the datasheet and was designed to be adjustable prior to putting the exoskeleton on. Because the magnet is embedded in a stainless steel shaft, which is slightly magnetic and could alter the magnetic field strength, the magnet standoff distance was adjusted in both directions until the signal failed, then located in the middle of this range. Prior experience showed that when ferrous materials are in close proximity, the standoff distance should be manually adjusted. The RM08 itself communicates with the Arduino using the SPI protocol over two digital pins. Its position is retrieved using a call function within the Arduino code which takes roughly 25-50 microseconds.

System Control and Testing, Discussion

4.1 Control

Next, the sensors and actuator were used together in a force controlled scheme. The controller diagram is shown again in Figure 19, with greater detail than previously. For clarity and intuition, sample values with appropriate units are shown between select elements.

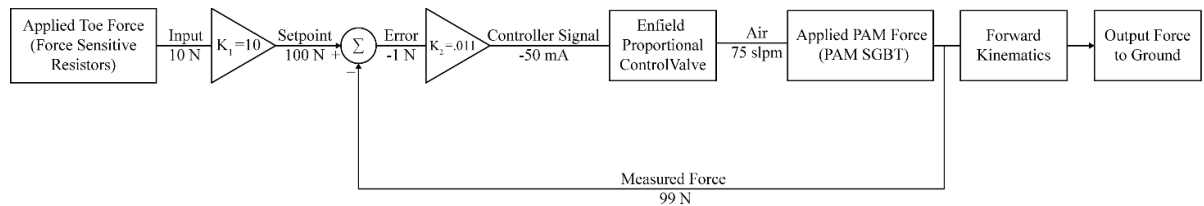


Figure 19. Detailed Controller Block Diagram

Unlike an electric motor, torque/force are not directly controlled, but rather flowrate. Therefore, error is roughly proportional (though non-linearly) to the derivative of force, assuming the object being pushed on is moving slowly relative to the bandwidth of the controller. This means that, unlike an electric actuator, steady state error is not proportional to force, but would ideally go to zero as air would continually fill the PAM. In reality, however, there is a deadband in the valve spool that still allows steady state error. The D1 driver has a trim pot to compensate for deadband, which helped to reduce, but not eliminate this. There is also hysteresis in the PAM itself, which contributes to steady state force error.

4.2 Testing

For testing, an arbitrary K_1 gain of 10 N/N was used. In other words, for an applied load of 1 N, the PAM would try and exert 10 N of force. Some exoskeletons refer to this gain as the “assist ratio”. A structure was built around the exoskeleton to allow it to press against the weight plate in a controlled manner. Initially, one of the FSRs was used to test the control system and determine an appropriate K_2 gain for a stable controller. After tuning, a gain of 1.3% full scale control signal per Newton of error was determined, i.e. at 77N of error or more, the valve would open fully. It was attempted to add a derivative term to dampen the system and allow a higher proportional gain, but this always caused greater instability without any impact on dampening the proportional term response. Additionally, it was attempted to associate the derivative term with the encoder output. However, this also led to instabilities, likely due to an inadequate resolution of 12 bits ($\sim 0.1^\circ$). A slight integral term was added to eliminate steady state error, with a windup limit of approximately 10% of the valve full-scale-output (FSO).

Figure 20 shows the response of the PAM to an FSR signal being pressed on arbitrarily with a finger. Recall that input force to the FSR was multiplied by $K_1 = 10X$ to generate the desired force trajectory, i.e. a physical force of only $\sim 20N$ was exerted against the FSR.

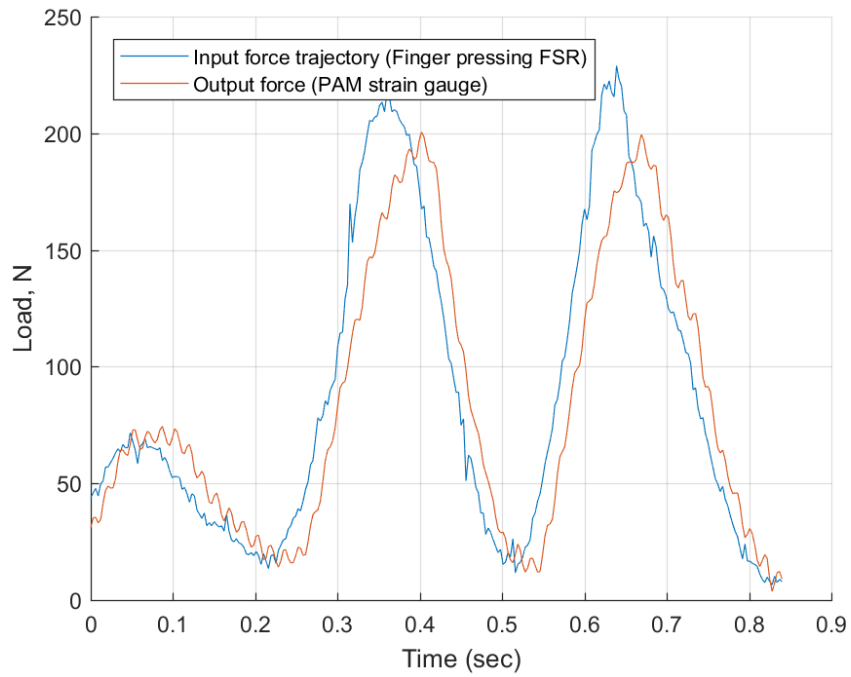


Figure 20. Control Input Response to Finger Pressing

Given the short timescale, the PAM follows the input trajectory very responsively. Next, a sine wave was generated to send a controlled time varying signal at

a higher speed than achievable by hand. A frequency of 5 Hz was selected, as this should encompass even a fast running gait force profile. Figure 21 shows the PAM response.

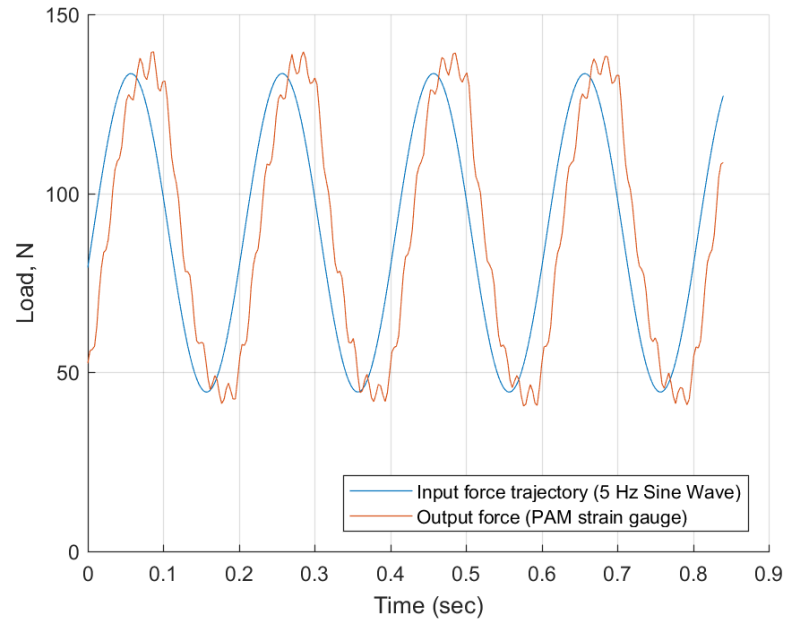


Figure 21. 5 Hz Sine Wave PAM Response

The PAM was able to keep up with the input signal at full amplitude, with roughly a 40° phase offset. Lastly, a square wave trajectory was generated to look at the

rise time and overshoot of the system. Figure 22 shows the PAM response to this trajectory.

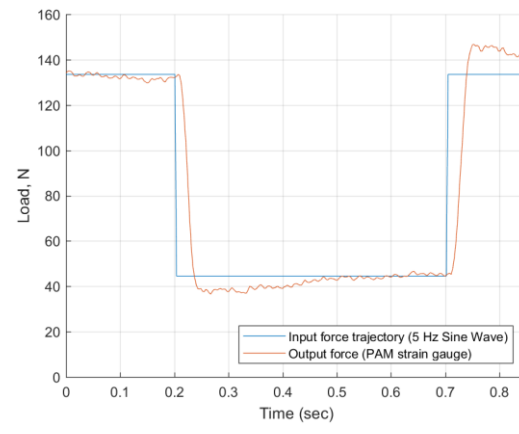
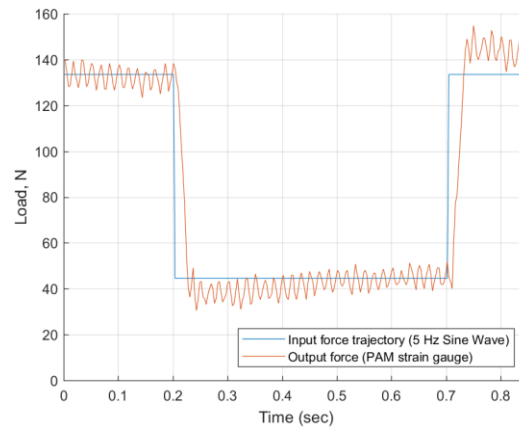


Figure 22. 1 Hz Square Wave PAM Response unfiltered (left), 5 sample mean filter (right)

4.3 Discussion

This step response yields a rise time of 21 milliseconds and a 9.2% overshoot.

Treating the response as a second order control system, we can use the equations

$$\zeta = \sqrt{\frac{\ln(OS)^2}{\pi^2 + \ln(OS)^2}} = 0.605 \quad (12)$$

$$\tau \approx \frac{t_r}{2.2} \approx 9.5 \text{ ms} \quad (13)$$

$$\omega_n = \frac{1}{\tau * \zeta} = 174 \frac{\text{rad}}{\text{sec}} = 27.7 \text{ Hz} \quad (14)$$

Where ζ is the damping coefficient, τ is the time constant, and ω_n is the natural frequency. The calculated natural frequency of 28 Hz is 9x faster than a high speed 3 Hz running gait. The latency sources contributing to this bandwidth are summarized in Table 3.

Table 3. Contributors to Control Bandwidth Response

Component	Delay Type	Latency	Reasoning
PAM SGBT / Structure	Mechanical	est. <<1ms	Natural frequency solid metal structure is very high
AD8426 Strain gauge amplifier	Electrical	0.1 ms	Dynamic response from datasheet [23] at gain of 500x [24]
Arduino control system	Processing	<1ms	Arduino control loop runs at 1000 Hz for all data acquisition, computation, and digital output;
BSS138 Logic level converter	Electrical	23 ns	From datasheet [25]
I2C comms	Communication protocol	est. <<1ms	48 bits per reading @ 100 kHz min [26]
MCP4725 DAC	Electrical	8 usec	Full scale rise/settling time

D1 Valve Driver	Electrical	est. $\ll 1$ ms	Datasheet does not publish response time. Typical current drivers are much faster than 1ms
LV25s Valve	Electro-mechanical	11ms	Datasheet value to cycle through all three valve positions [17]
PAM Inflation	Pneumatic	Tbd	Volume/flowrate estimate

As seen from Table 3, there are two sources of latency that dominate the system bandwidth – the bandwidth of the valve as well as the pneumatic response of the actuator. Combining all other sources of latency leaves approximately 20 ms of latency for these two contributors. The first major contributor is the valve bandwidth, which the datasheets claim is 88 Hz, or 11 ms, to complete one full cycle across the entire stroke of the spool. This value is likely longer than in reality, as the valve does not need to travel the entire spool distance to open the orifice. Rather, one quarter of this time can be used, the time it takes the spool to go from centered (where it was at the last force setpoint), to fully open. This would give a latency of 2.7 ms.

To estimate the latency of the PAM filling, the PAM volume is modeled as a constant volume cylinder with a changing pressure. This is because the leg was locked in place, so the ankle did not rotate. Even though this may not seem representative of a realistic use case, one must recall that most of the airflow through the valve should be analyzed in standard liters per minute (SLPM), which is measured at standard temperature and pressure (STP). Changing the geometric volume of the PAM (i.e. changing the stroke) and maintaining a constant pressure requires far less air at STP than drastically changing the pressure (i.e. changing the force). This is because pressure and force are

roughly proportional to each other. We can therefore estimate the volume of air required at STP for the step input in Figure 22:

$$V_{i,STP} = \frac{p_i \cdot V_i}{p_{i,STP}} = \frac{1.35 \text{ bar} \cdot 420 \text{ cc}}{1.01 \text{ bar}} = 561 \text{ cc} = 0.56 \text{ liters} \quad (15)$$

$$V_{f,STP} = \frac{p_f \cdot V_f}{p_{f,STP}} = \frac{2.04 \text{ bar} \cdot 420 \text{ cc}}{1.01 \text{ bar}} = 848 \text{ cc} = 0.85 \text{ liters} \quad (16)$$

$$\Delta V_{STP} = V_{F,STP} - V_{I,STP} = 0.29 \text{ liters} \quad (17)$$

Where ΔV_{STP} is the amount of air at STP that must flow through the valve for the desired force setpoint to be achieved. To solve for this volume, we must know the initial and final *absolute* pressure of the PAM, as well as the total volume after the cylinder. Looking at the LV-25s datasheet [17] shown in Figure 23, graphical information is given showing the relationship between output flow and differential pressure.

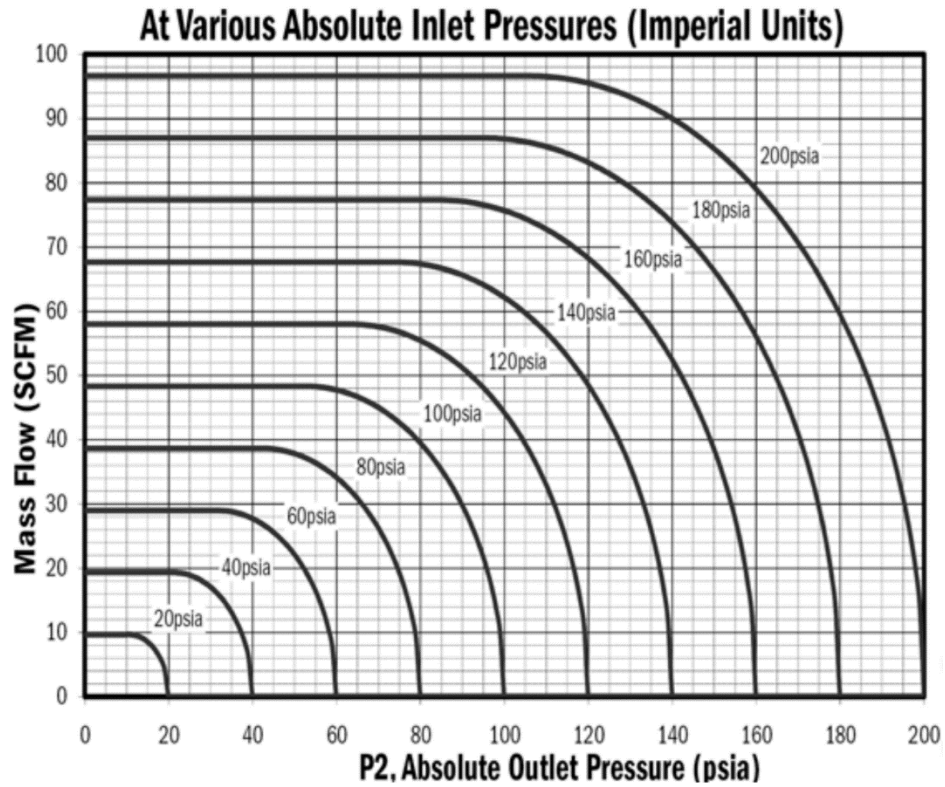


Figure 23. LS-V25s Mass Flow vs. Outlet Pressure

At an inlet pressure of 50 psia (3.45 bar), the output flow remains relatively constant throughout the pressure increase at the PAM to 29 psi (2.0 bar). This flowrate is approximately 700 lpm. Therefore, it should theoretically take approximately

$$t_{fill} = \frac{Q_{valve,STP}}{\Delta V_{STP}} * 60 \frac{\text{seconds}}{\text{minute}} = \frac{700 \text{ lpm}}{0.29 \text{ liters}} * 60 \frac{\text{seconds}}{\text{minute}} = 25 \text{ ms} \quad (18)$$

To fill the PAM and achieve the change in force. Obviously, this is impossible because the rise time was only 21 milliseconds. However, this is only a rough order of magnitude (ROM) estimate and contains many sources of error that are difficult to bound. The largest sources of error are (A) the initial and final pressure, which had to be estimated because pressure sensors were not present. The estimate assumes a linear pressure vs. force relationship. (B) PAM volume was estimated by multiplying the PAM diameter by its length, which does not take into account the end necking regions, making this estimate likely too high. If this were lower, the estimated response time would also have been lower. (C) Valve flowrate was estimated graphically using data that assumes a fully open orifice. In reality, the orifice is controlled by the PID loop, which closes itself when the setpoint is nearly reached, and also requires several milliseconds to fully open, as discussed earlier. Some combination of these error sources are the cause for the estimated fill time being longer than the actual rise time of the system.

Nonetheless, ROM estimates can still be very useful and this analysis is no exception. Comparing the pneumatic fill time of the system (25 ms) to the valve quarter-bandwidth (2.7 ms), as well as to all the other sources of latency (~1 ms), shows that the pneumatic dynamics are most likely the driver for system control frequency. Even if the sources of error are off by a factor of 200% or more, the pneumatic dynamics still drive

the control frequency. This comes as no surprise, as pneumatics are historically known to be extremely hard to control relative to electric and hydraulic systems.

Conclusions, Future Work

5.1 Conclusions

The system exhibited a controlled bandwidth of 28 Hz, which is 9x faster than a high speed 3 Hz running gait. This frequency is suitable for a dynamic exoskeletal application. Though this was a simple benchtop test setup, it showed that the combination of sensors, actuators, control valve, and control electronics are capable of end-to-end supporting said frequency within a portable package. When using a PAM for an exoskeletal application, it is absolutely essential to use a proportional valve if high bandwidth control is desired. The control precision and frequency response would not have been achievable with simple two-state solenoid valves.

If one wanted to increase the control frequency, there would be several ways to do so. (1) The most effective way to do this would be to increase the flow capacity of the valve. Realistically, however, the valve is already the single heaviest, non-mechanical component as is, and would begin to impact overall mass drastically as it increases in size. (2) One could also decrease the volume downstream of the valve. If the PAM were to have a filled center with a telescoping sealed rod, the working volume would be drastically reduced. This would not only increase control frequency, but decrease compressed air consumption, extending life. A tangentially designed hybrid PAM is shown in Appendix B - Hybrid PAM Concept. (3) Lastly, if the system pressure were to be increased, and the PAM working pressure held constant, the flowrate through the

valve would increase, thus increasing control frequency. This is made especially clear looking at Figure 23.

The second major focus of this thesis was the proprioception. As discussed earlier, force sensitive resistors were shown to exhibit adequate dynamic response and low hysteresis characteristics suitable for a high bandwidth control scheme. Their linearity and repeatability is not at the same level as commercial strain gauge based force sensors, but they are the best sensor available in their form factor class. By increasing the number of FSRs on the foot to provide coverage, it is likely that accuracy, reliability, and robustness to non-uniform loading would increase drastically. The SGBT embedded in the PAM also proved to have performance capabilities adequate for closed loop control. The system was highly stable while maintaining an extremely fast response rate suitable for exoskeletal applications.

The combined actuator-proprioeption-electromechanical system investigated and proved several useful technologies in conjunction with each other. Though applied to a 1-DOF benchtop exoskeleton, these findings show a great deal of promise for applications extending into full lower body exoskeletons with dynamic locomotion capabilities.

5.2 Future Work

The most essential future work to do is to redesign or stiffen the primary structure to handle higher PAM loads. This will allow the exoskeleton to operate in the regime of highly dynamic, 2g+ loads. Following that, the exoskeleton could actually be worn and tested.

Subsequently, state management and gait recognition algorithms would be required to synchronize the exoskeleton control modes with the walking, running, or jumping gait. Though the ankle encoder was used minimally in this research effort, it would be absolutely essential in an actual running or jumping application. It is likely an IMU would also need to be added because the wearer's orientation is not always known relative to the ground.

The system currently runs off of an off-board power source. As discussed earlier, a compressed air source such as a paintball tank would be necessary to make the system fully portable.

Longer term, much of the hardware could be upgraded to be more robust and representative of a commercial device. Examples of this include embedding the FSRs into an insole, more robustly integrating the SGBT into the PAM (hermetic sealing, strain relief, etc.), further embedding I/O electronics, and lightweighting the control valve.

These changes would extend the impact and usefulness of this research effort, bringing highly dynamic pneumatic exoskeleton technology closer to the commercial market.

Appendix A - Source Code

Arduino Source Code

```
#include <PID_v1.h>
#include <Wire.h> //Include the Wire library to talk I2C
#define MCP4725_ADDR 0x60

//Primary inputs for easy access
int data[8]; //PAM Strain, Weight plate, Outer side FSR, Middle
FSR, Inner side FSR, Encoder, PID Setpoint, PID Input (Angle)
const int ch = 4;
unsigned long tLoop = 1000; // Length of loop in microseconds
int logRate = 2; // Length of data logging loop, in ms. Should be a
multiple of the tLoop length after converting units
double preload = .5; // Target preload to push against the toe with
double amp = 10; // Amplitude of sine wave for testing
double ofst = 20; //Offset of sine wave for testing
double tm = 1000.0; //unitless time (no of loop iterations actually)
to complete one sine wave for testing
int timer = 0; //Used to send time signal to matlab
int startTime = 0; //For offset in time signal

// Encoder info
const int CLOCK_PIN = 5;
const int DATA_PIN = 6;
const int BIT_COUNT = 12;
const int bufSz = ch*2;
byte buf[bufSz];
int angle = 0;

//Valve Stuff
int valveCenter = 1928; // Used to be 2159/4095 for 2.5V empirically
determined with multimeter, but changed instead to where the valve
started allowing return pressure through

// PID Variables
bool actuate = true; // If set to true, Arduino will compute PID and
send valve commands
double P = 125;
double I = 1;
double D = 0;
double err = 0;
double Setpoint = 0;
double Input = 0;
double Output = 0;
double valveCmd = 0;
double releaseGain = 10; // Additional vain factor so PAM releases
faster than it contracts
double beta = 0; // Angle input for sine wave for testing
int cnt = 0; //Count for iterating through sine wave for
testing
const int avgLen = 5; //Number of samples to average to determine
velocity
int vels[avgLen]; //contains all the velocities
```

```

double vel = 0;           //contains current velocity, in arbitrary
units
int avgInd = 0;          //Location of current velocity index
int lastPos = 0;         //Contains last position of angle encoder for
estimating velocity
double integral = 0;     // For calculating integral term
int windup = 500;       // Max windup allowable, relative to max
control signal of 4096

//Timing Variables
unsigned long start = 0;
int tooSlow = 0;        // Bool to tell when Arduino can't keep up
with loop rate
int logCnt = (int)(1000 * logRate / tLoop); //for counting to logRate

// int zeros[] = {1405,3828,0,0,0,900}; // PAM load cell, Weight plate,
FSR1, FSR2, FSR3, Encoder
int zeros[] = {1448, 4005, 0, 0, 0, 900, 0, 0};
double scaling[] = {.12, -.1, .0103, .00922, .0107, 1, 1, 1, 1};
double FSRs[] = {0, 0, 0};
double fFSRs = 0;
double fPlate = 0;
double fPAM = 0;

void setup()
{
  // Encoder setup
  pinMode(DATA_PIN, INPUT);
  pinMode(CLOCK_PIN, OUTPUT);
  digitalWrite(CLOCK_PIN, HIGH);

  // PID Setup
  //initialize the variables we're linked to
  Input = analogRead(0);
  Setpoint = 100;
  lastPos = readPosition();
  for (int i = 0; i<avgLen; i++){
    vels[i] = 0;
  }

  // Board Setup
  Serial.begin(115200);
  analogReadResolution(12);
  analogWriteResolution(12);
  analogWrite(DAC0, (int)valveCenter);
  start = micros();
  Wire.begin();

  // Use LED to tell when arduino can't keep up
  pinMode(13, OUTPUT);
  digitalWrite(13, LOW);
  startTime = millis();
  delay(500);
}

void loop()
{

```

```

if (micros() - start > tLoop){
  if (!tooSlow){
    start = start + tLoop;
    digitalWrite(13, LOW);
  } else {
    start = micros();
    digitalWrite(13, HIGH);
  }
  tooSlow = 1;

  // Read selected sensors
  data[0] = analogRead(A1); // Read PAM strain gauge
  data[1] = analogRead(A0); // Read weight plate
  data[2] = analogRead(A4); // Read FSR #1 (Outer)
  data[3] = analogRead(A3); // Read FSR #2 (Middle)
  data[4] = analogRead(A5); // Read FSR #3 (Inner)
  data[5] = readPosition();

  //Process readings
  FSRs[0] = (data[2]-zeros[2])*scaling[2];
  FSRs[1] = (data[3]-zeros[3])*scaling[3];
  FSRs[2] = (data[4]-zeros[4])*scaling[4];
  fFSRs = (FSRs[0]+FSRs[1]+FSRs[2])*4-preload; // Estimated FSR
force based off of combined sensor data, with preload offset applied
  fPAM = (data[0]-zeros[0])*scaling[0]; //Calculate PAM force
  fPlate = (data[1]-zeros[1])*scaling[1]; //Calculate weight plate
force

  //Estimate velocity
  vel = vel - (double)vels[avgInd]/(double)avgLen;
  vels[avgInd] = fPAM-lastPos;
  lastPos = fPAM;
  vel = vel + (double)vels[avgInd]/(double)avgLen;
  avgInd++;
  avgInd = avgInd % avgLen;

  if (actuate){
    // For sending sine or square wave signal
    //cnt = cnt + 1;
    //if (cnt >=(int)tm) cnt=0;
    //beta = cnt/tm;
    //Setpoint = amp*sin(2*3.141592*beta)+ofst; // Sine signal
    //if (beta >.5){
    //  Setpoint = ofst+amp;
    //} else {
    //  Setpoint = ofst-amp; // Square wave signal
    //}

    Setpoint = (FSRs[0]-preload)*10;
    Input = fPAM;
    err = Setpoint - Input;
    integral = constrain(integral + err, -windup, windup);

    Output = err * P + integral * I - vel*D;
    if(Output<0){ valveCmd = Output*releaseGain; // i.e. PAM is
extending
      }else{ valveCmd = Output; }
  }
}

```

```

    valveCmd = constrain(valveCenter-(int)Output, 0, 4095);
    int temp = floor(valveCmd);
    Wire.beginTransaction(MCP4725_ADDR);
    Wire.write(64); // cmd to update the DAC
    Wire.write(temp >> 4); // the 8 most significant bits...
    Wire.write((temp & 15) << 4); // the 4 least significant bits...
    Wire.endTransmission();
    Output = valveCmd - valveCenter;
}

// Data Logging, only every once in a while
logCnt = logCnt + 1;
timer = millis()-startTime;
if (logCnt>logRate && timer > 1000){
    logCnt = 0;
    buf[0] = (int)(timer) & 255;
    buf[1] = ((int)(timer) >> 8) & 255;
    buf[2] = (int)(fPAM*100) & 255;
    buf[3] = ((int)(fPAM*100) >> 8) & 255;
    buf[4] = (int)(Setpoint*100) & 255;
    buf[5] = ((int)(Setpoint*100) >> 8) & 255;
    buf[6] = (int)(fPlate*100) & 255;
    buf[7] = ((int)(fPlate*100) >> 8) & 255;
    //buf[8] = (int)(Output) & 255;
    //buf[9] = ((int)(Output) >> 8) & 255;
    Serial.write(buf, sizeof(buf));
}
} else { tooSlow = 0; }
}
// ***** HELPER FUNCTIONS BELOW HERE *****
//read the current angular position
int readPosition() {
    // Read the same position data twice to check for errors
    unsigned long sample1 = shiftIn(DATA_PIN, CLOCK_PIN, BIT_COUNT);
    delayMicroseconds(25); // Clock mus be high for 20 microseconds
    before a new sample can be taken, originally 25
    // unsigned long sample2 = shiftIn(DATA_PIN, CLOCK_PIN, BIT_COUNT);
    return sample1;
}
//read in a byte of data from the digital input of the board.
unsigned long shiftIn(const int data_pin, const int clock_pin, const
int bit_count) {
    unsigned long data = 0;
    for (int i=0; i<bit_count; i++) {
        data <<= 1;
        digitalWrite(clock_pin, LOW);
        delayMicroseconds(1); //originally 1
        digitalWrite(clock_pin, HIGH);
        delayMicroseconds(1); //originally 1

        data |= digitalRead(data_pin);
    }
    return data;
}
}

```

Matlab Source Code

```
% This code is designed to collect data from an Arduino over a serial
% connection. Written by Josh Geating, Oct. 2017

%% Arduino Setup
s = serial('COM4'); % change the COM Port number as needed
set(s,'BaudRate',115200, 'InputBufferSize', 512);
fclose(instrfind);
try
    fopen(s);
catch err
    fclose(instrfind);
    error('Error connecting to Arduino');
end

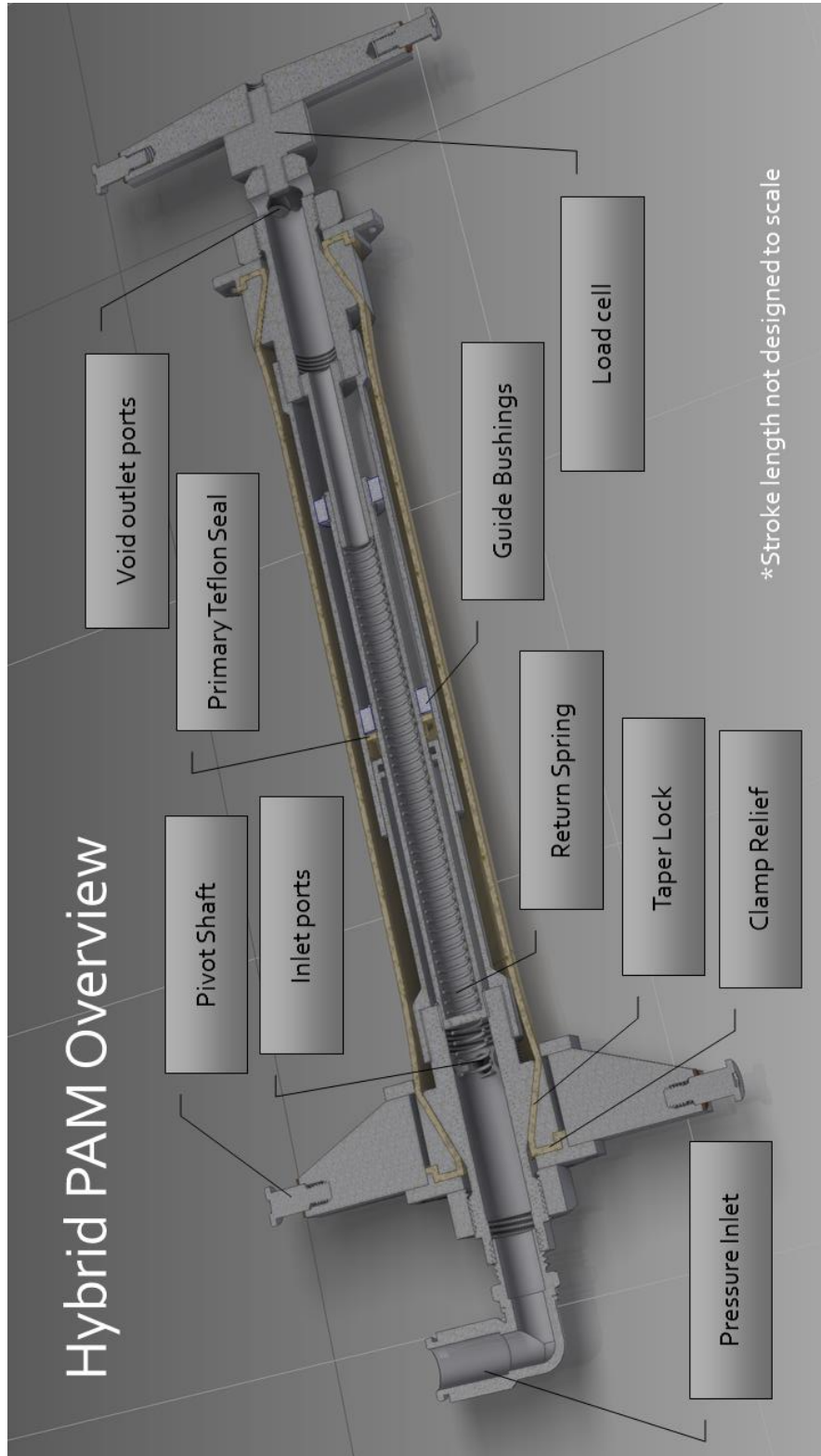
%% Set up figure for Live plotting
Tmax = 10; % Total time for data collection (s)
figure(1);
clf;
grid on;
xlabel('Time (s)'), ylabel('Data (16-bit)'),
% axis([0 3 0 20000]);

%% Read and plot the data from Arduino
% Data format is in a stream of 2-byte values, serially. Current format (subject to
% change):
% 1. PAM strain gauge
% 2. Weight plate
% 3. FSR #1: outer side
% 4. FSR #2: center
% 5. FSR #3: inner side
% 6. Encoder
% Data is raw, unscaled, with zero offsets. Variables created below to
% calibrate data to each other, and offset/scaling is performed realtime as
% data is received.

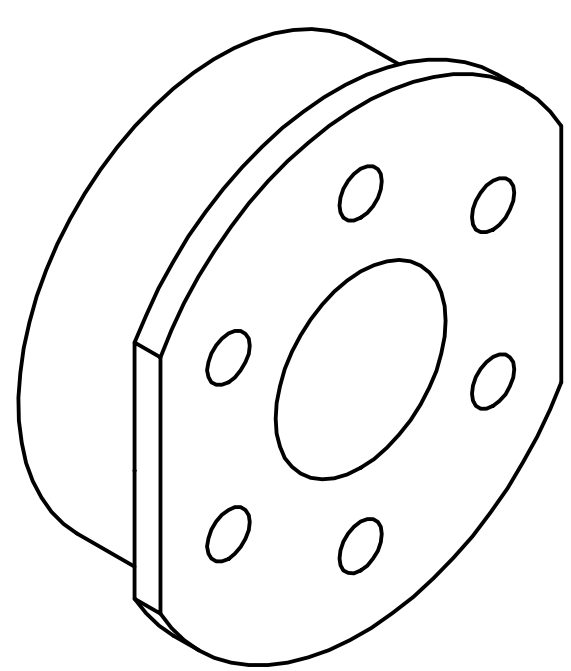
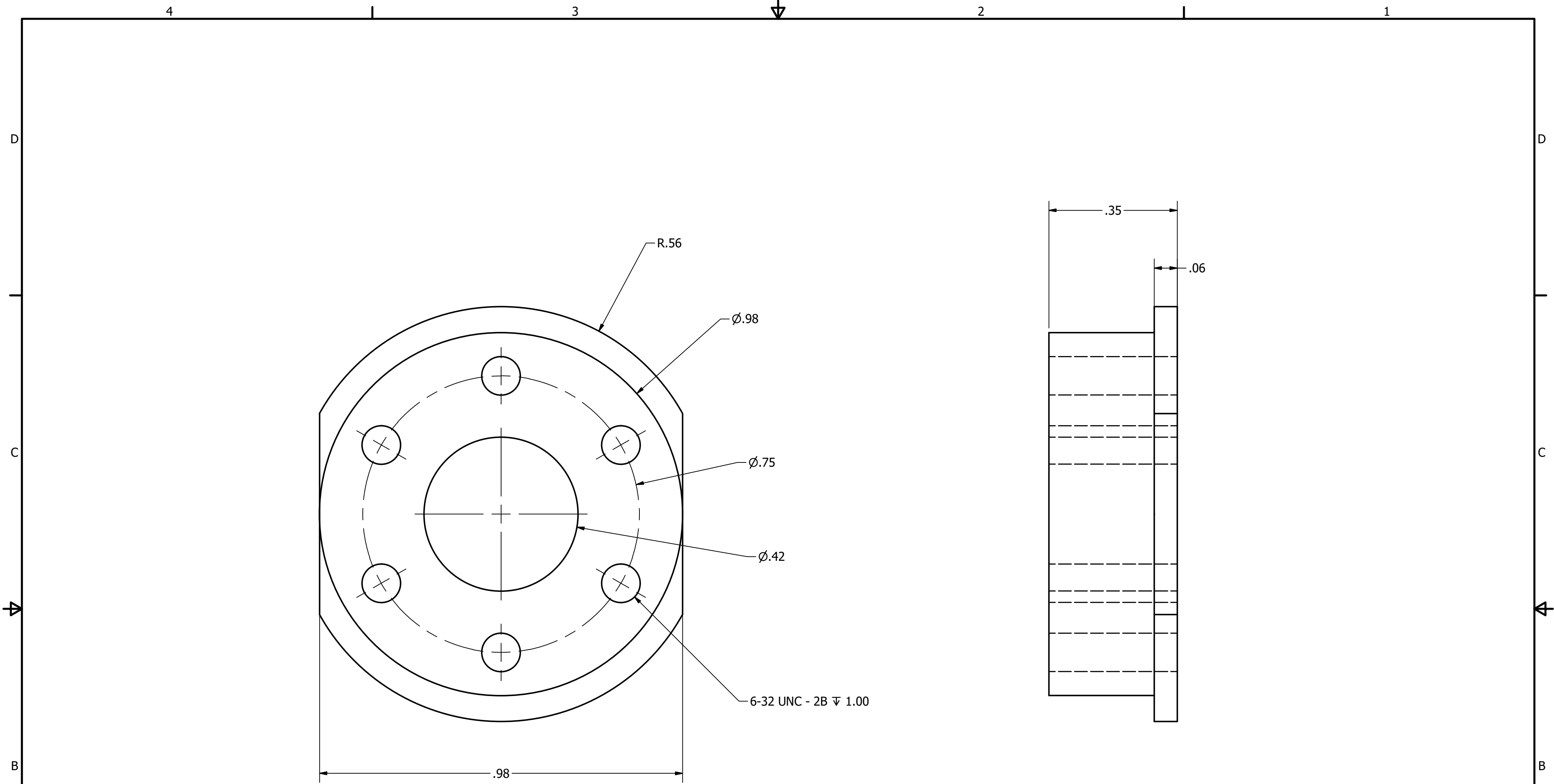
i = 0;
ch = 4;
data = zeros(5000, ch);
data2 = 0;
t = 0;
tic % Start timer
toofast = 0;
% scaling = [1 -.1 .0103 .00922 .0107 1 1 1]; % scaling factors
% offsets = [0 3824 0 0 0 900 0 0];
scaling = [1, 1, 1, 1];
offsets = [0, 0, 0, 0];
figure(1);
while toc <= Tmax
    i = i + 1;
    data(i, :) = (fread(s,ch,'int16') - offsets) .* scaling';

    if i > 2
        % line([tm(i-1) tm(i)], [data(i-1, 1) data(i, 1)], 'Color', 'red');
        line([data(i-1, 1) data(i, 1)]/1000, [data(i-1, 2) data(i, 2)]/100, 'Color',
'red');
        line([data(i-1, 1) data(i, 1)]/1000, [data(i-1, 3) data(i, 3)]/100, 'Color',
'green');
        % line([data(i-1, 1) data(i, 1)]/1000, [data(i-1, 4) data(i, 4)]/100, 'Color',
'blue');
        % line([data(i-1, 1) data(i, 1)]/1000, [data(i-1, 5) data(i, 5)], 'Color',
'cyan');
        drawnow;
    end
end
fclose(s);
```

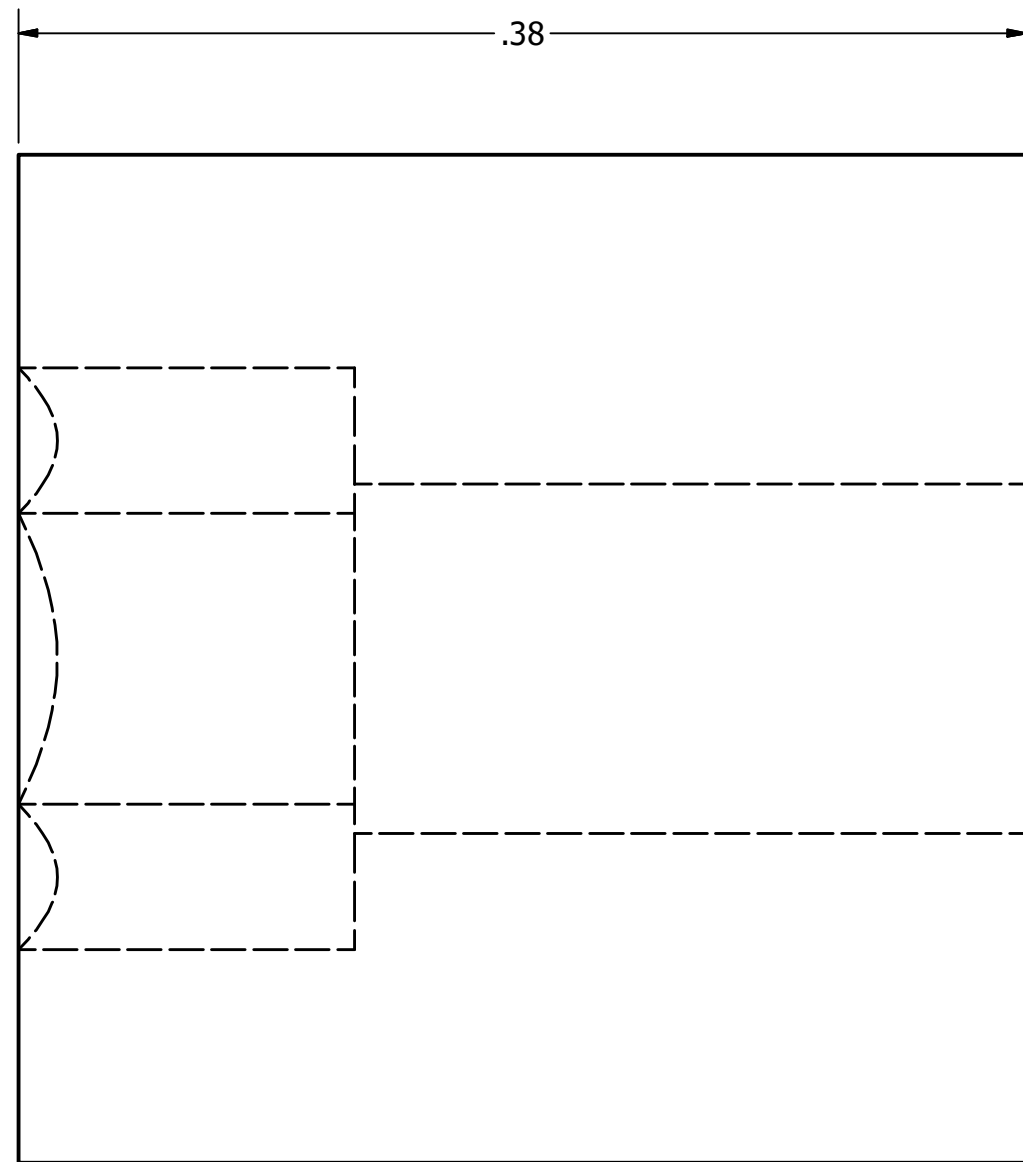
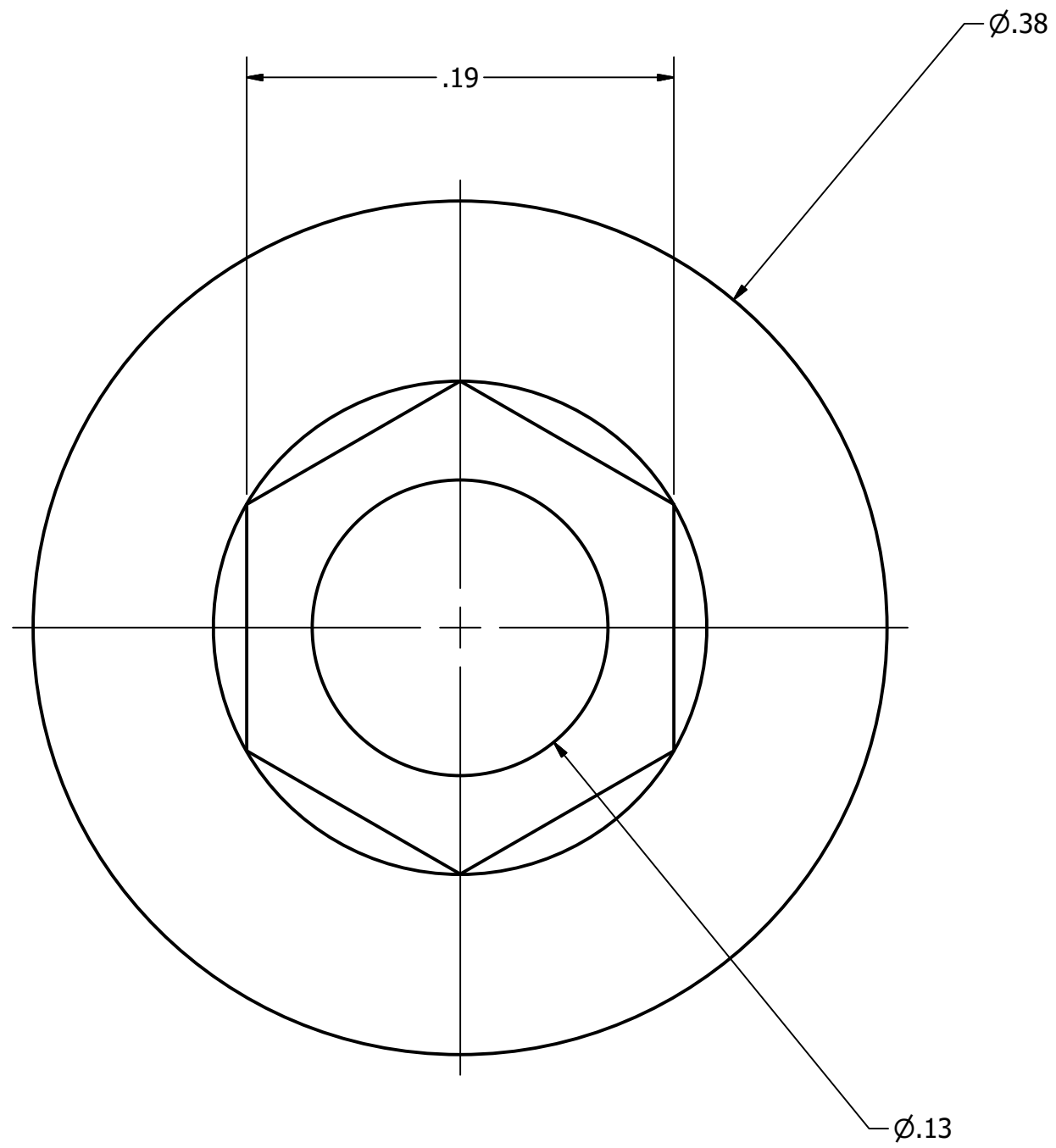
Appendix B - Hybrid PAM Concept



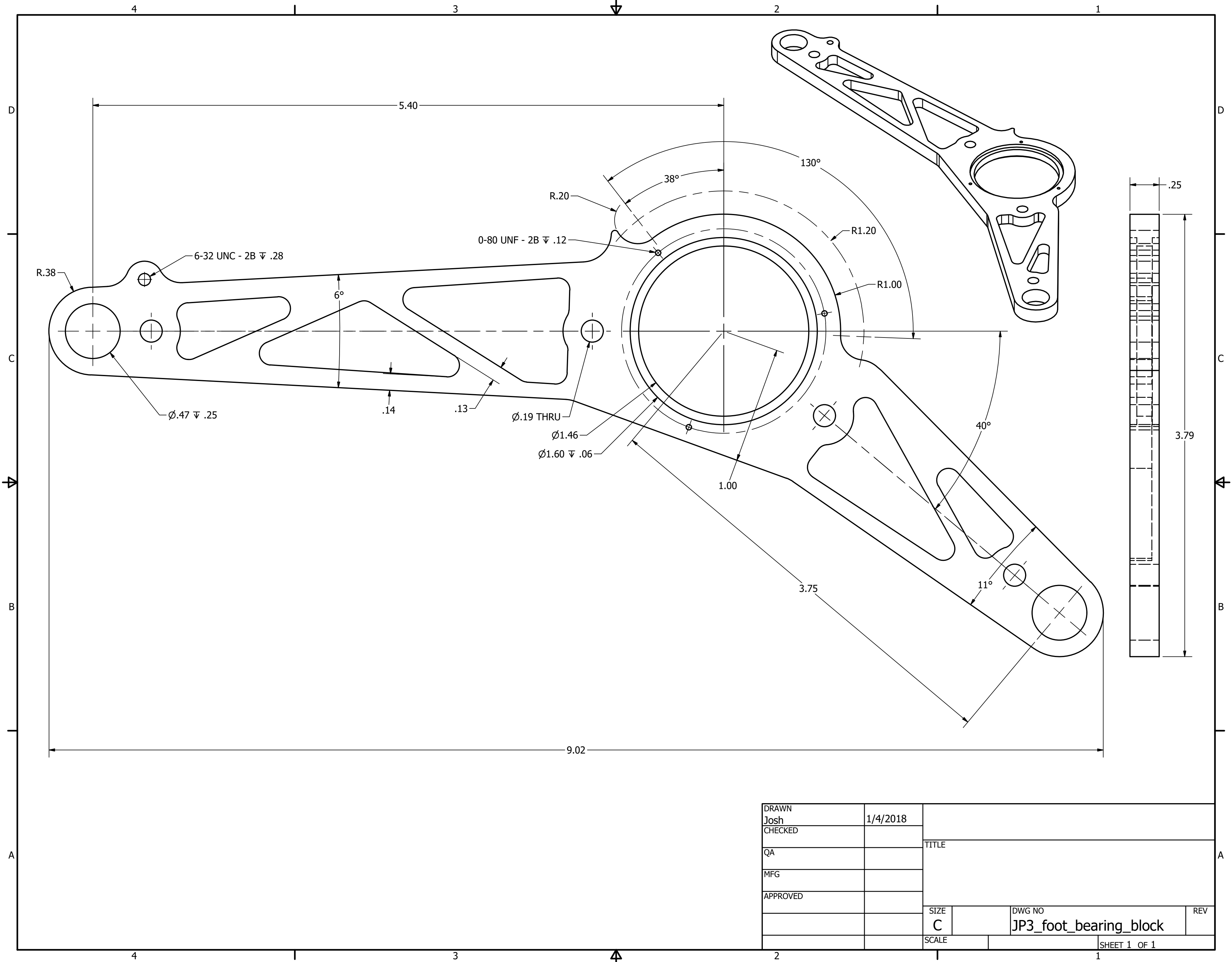
Appendix C - Mechanical Drawings



DRAWN Josh	1/4/2018	TITLE		
CHECKED				
QA				
MFG				
APPROVED		SIZE C	DWG NO ankle_shaft	REV
		SCALE	SHEET 1 OF 1	



DRAWN Josh	1/4/2018	TITLE		
CHECKED				
QA				
MFG				
APPROVED		SIZE C	DWG NO Anklee Hardstop - mcmaster modified	REV
		SCALE	SHEET 1 OF 1	



DRAWN	1/4/2018		
Josh			
CHECKED		TITLE	
QA			
MFG			
APPROVED			
		SIZE	DWG NO
		C	JP3_foot_bearing_block
		SCALE	REV

4

3

2

1

D

C

B

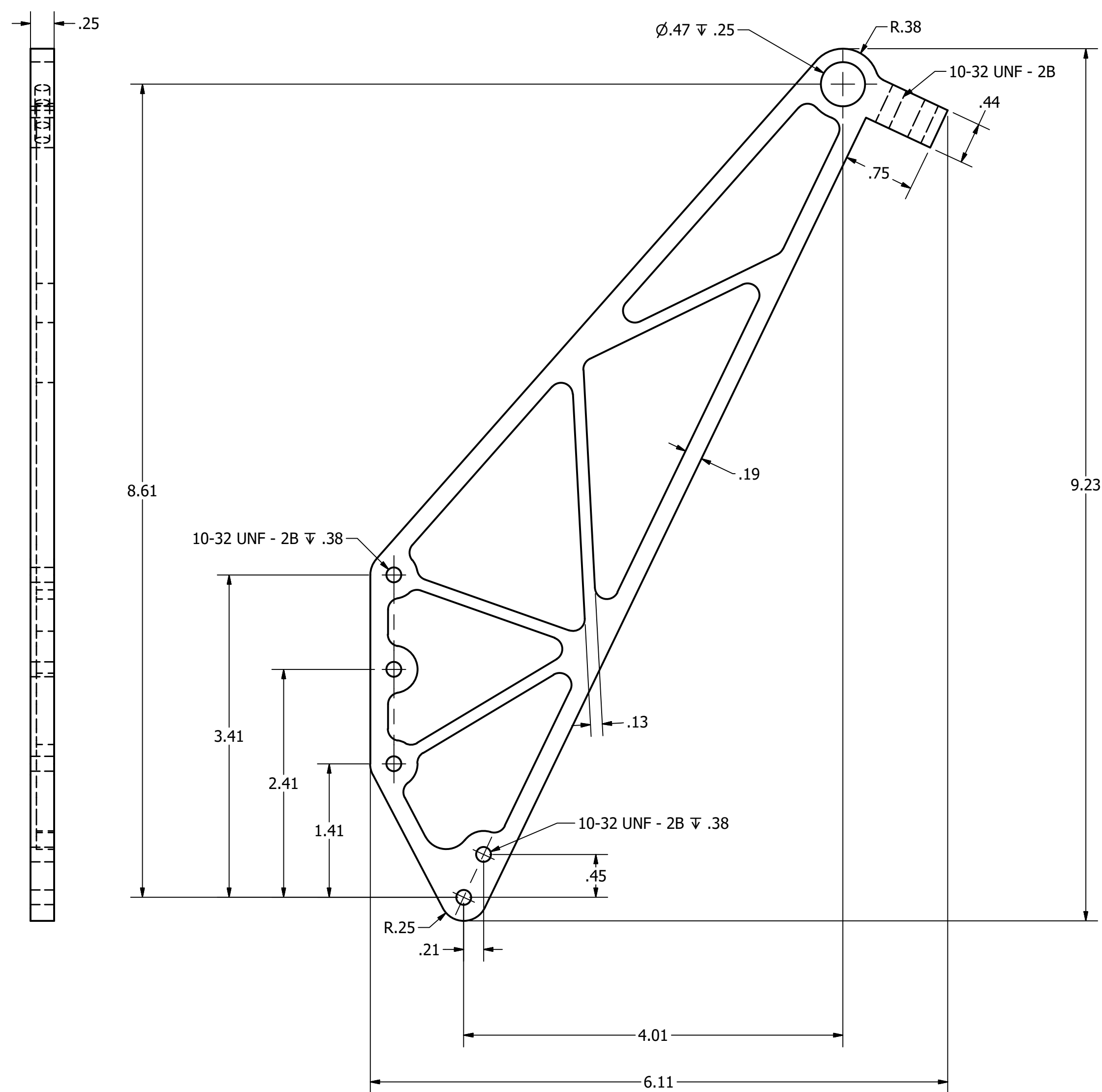
A

D

C

B

A



DRAWN Josh	1/4/2018	TITLE		
CHECKED				
QA		SIZE C		
MFG				
APPROVED		DWG NO JP3_PAM_Sideplate		REV
		SCALE		SHEET 1 OF 1

4

3

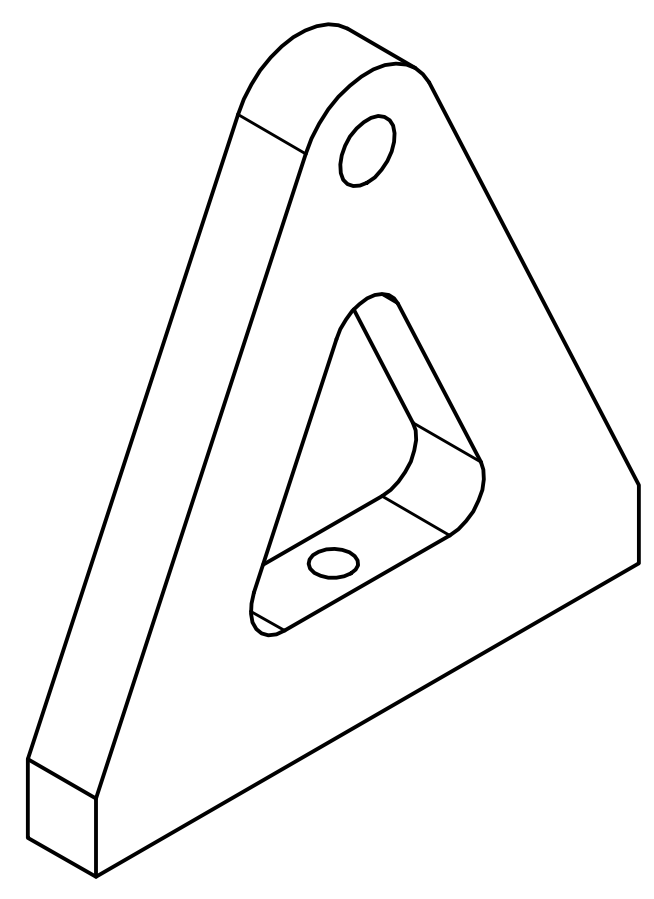
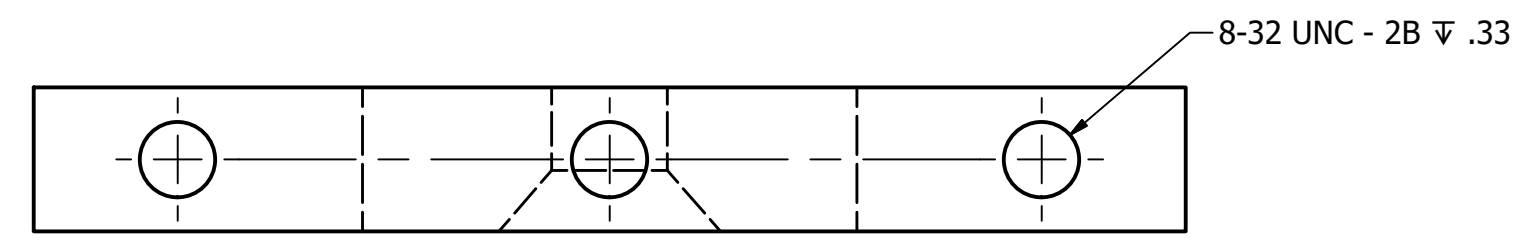
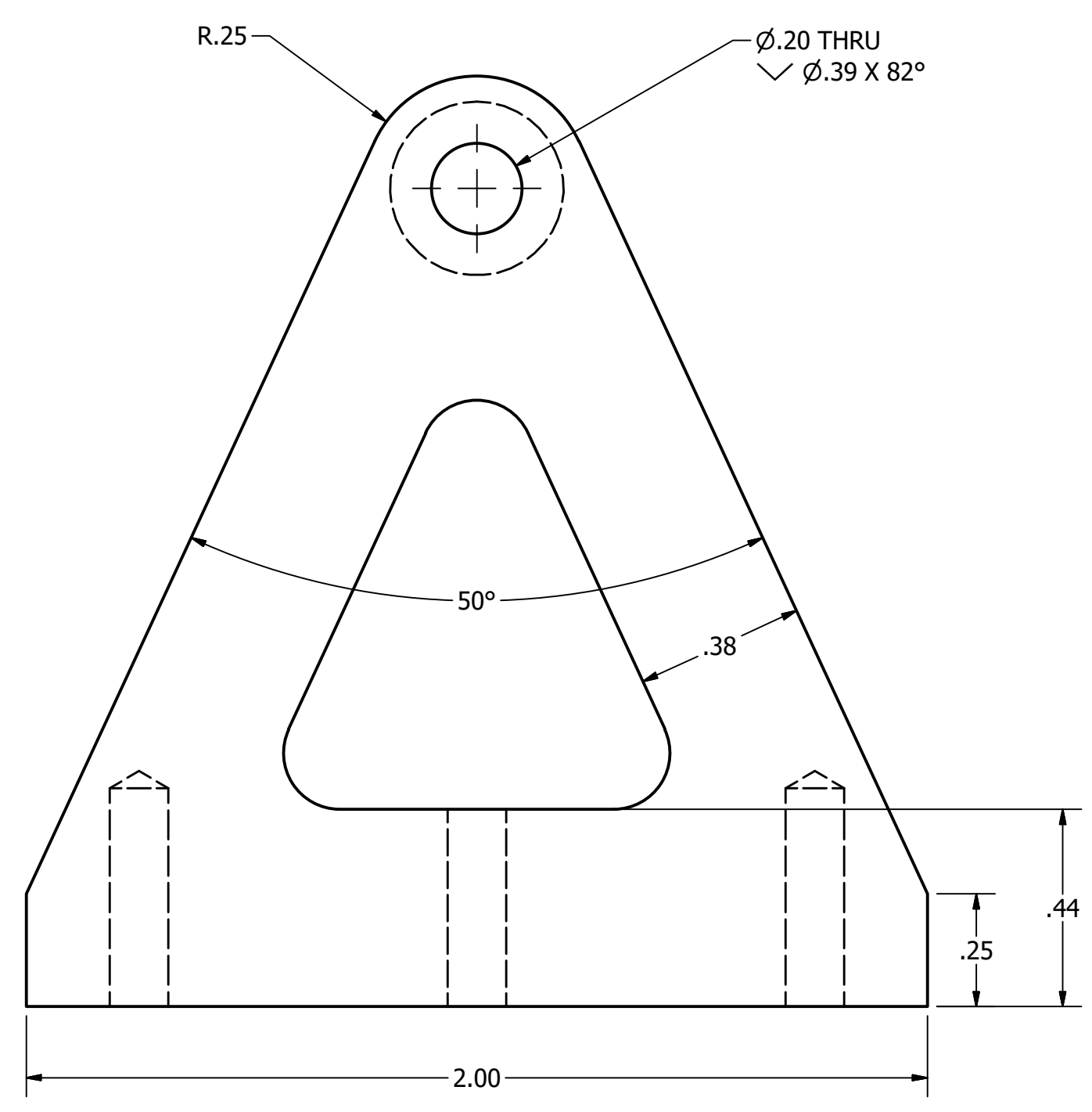
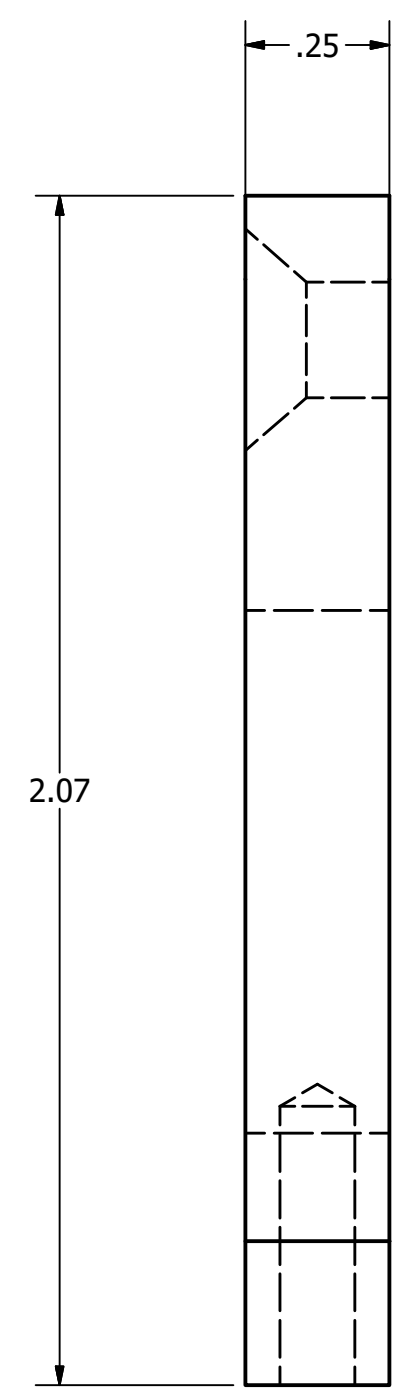
2

1



4 3 2 1

D C B A



DRAWN Josh	1/4/2018	TITLE		
CHECKED				
QA		SIZE C		
MFG				
APPROVED		DWG NO JP3_side_plate_anchor2		REV
		SCALE		SHEET 1 OF 1

4 3 2 1

D C B A

4 3 2 1

D

D

C

C

B

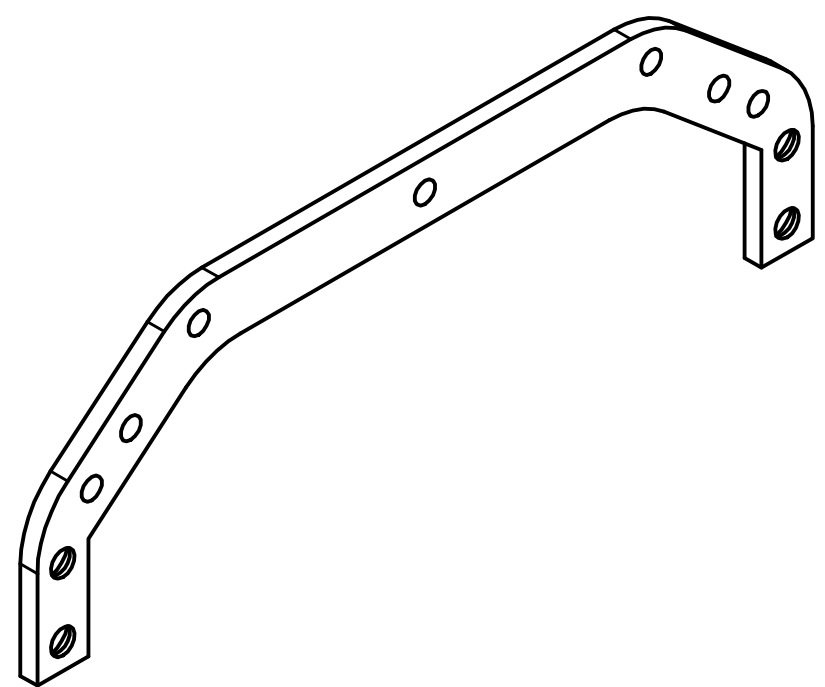
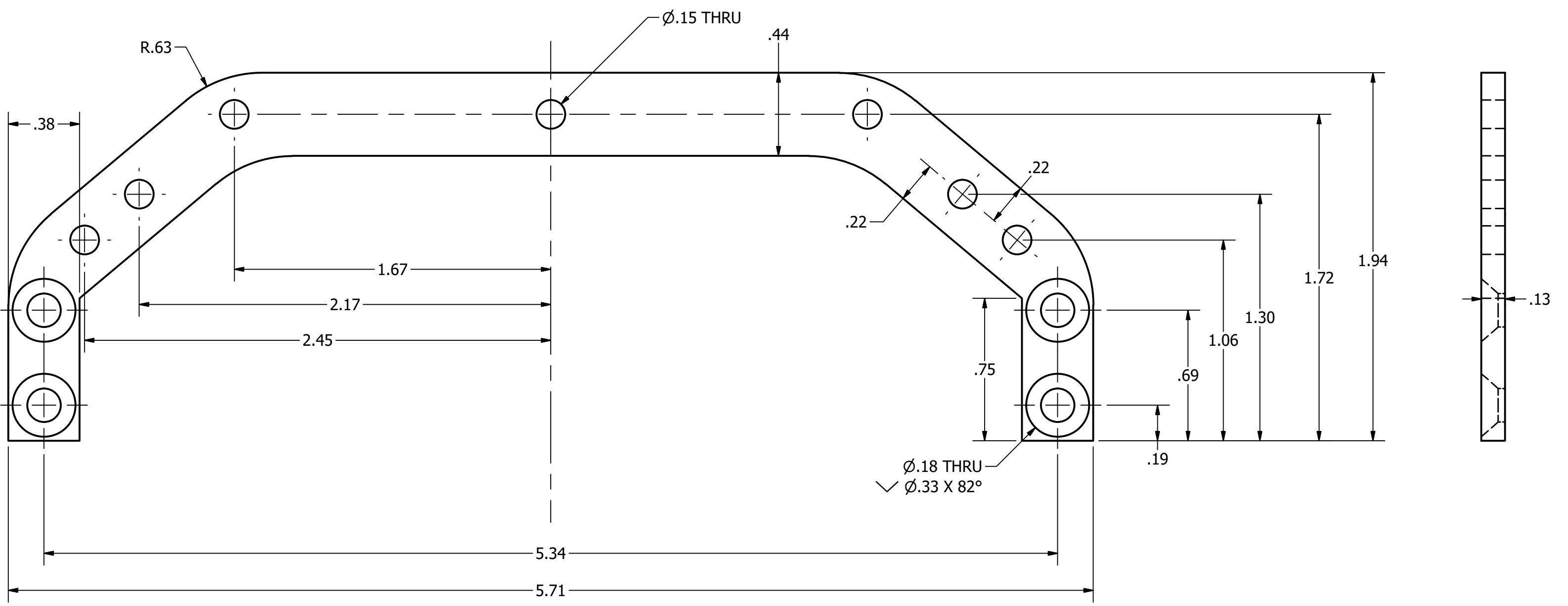
B

B

B

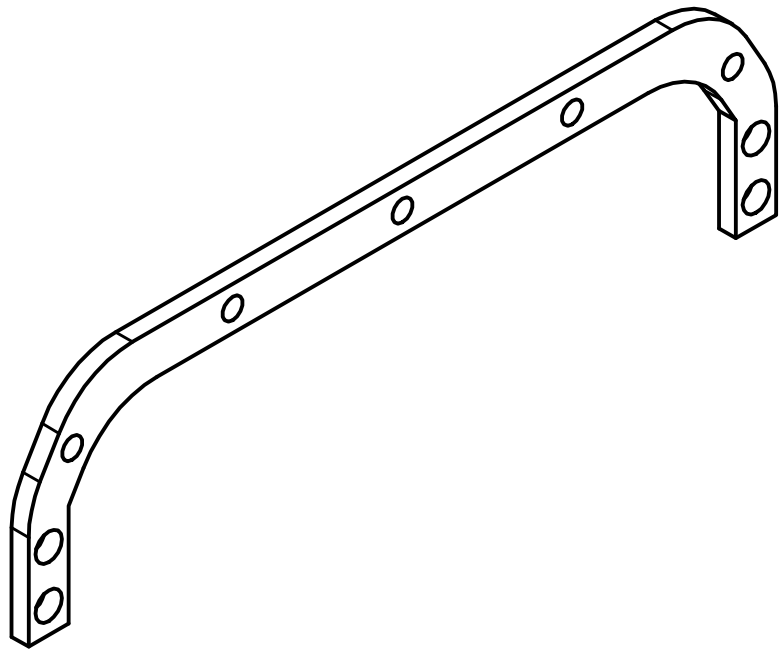
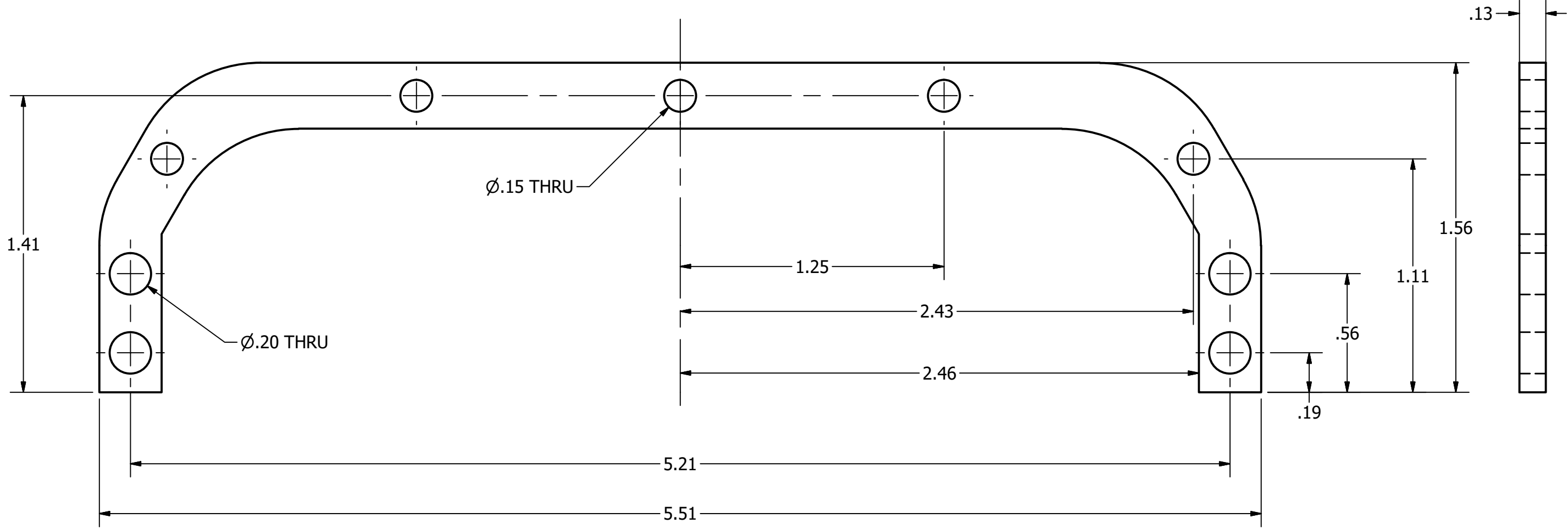
A

A



DRAWN Josh		1/4/2018		TITLE	
CHECKED					
QA					
MFG					
APPROVED				SIZE C	DWG NO JP3_Stiffener 2
				SCALE	SHEET 1 OF 1
				REV	

4 3 2 1

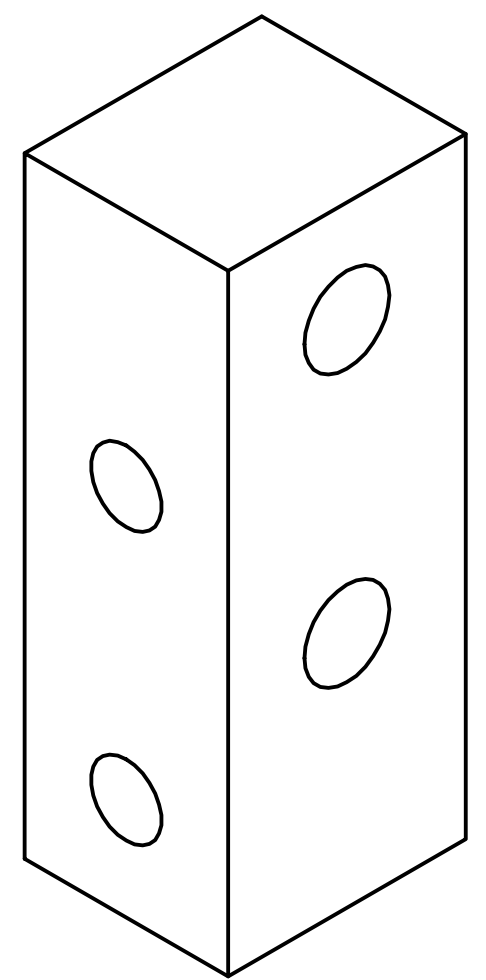
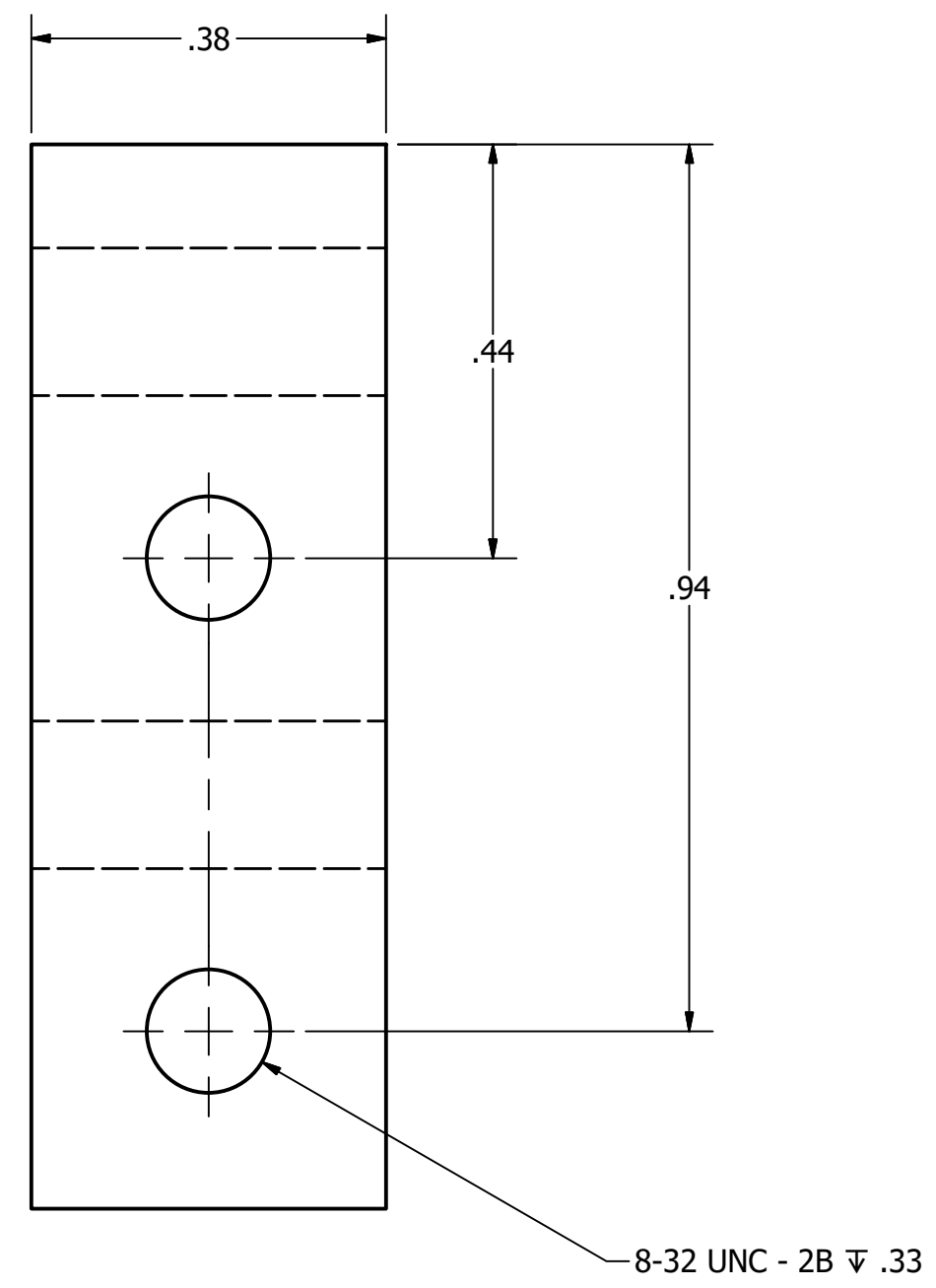
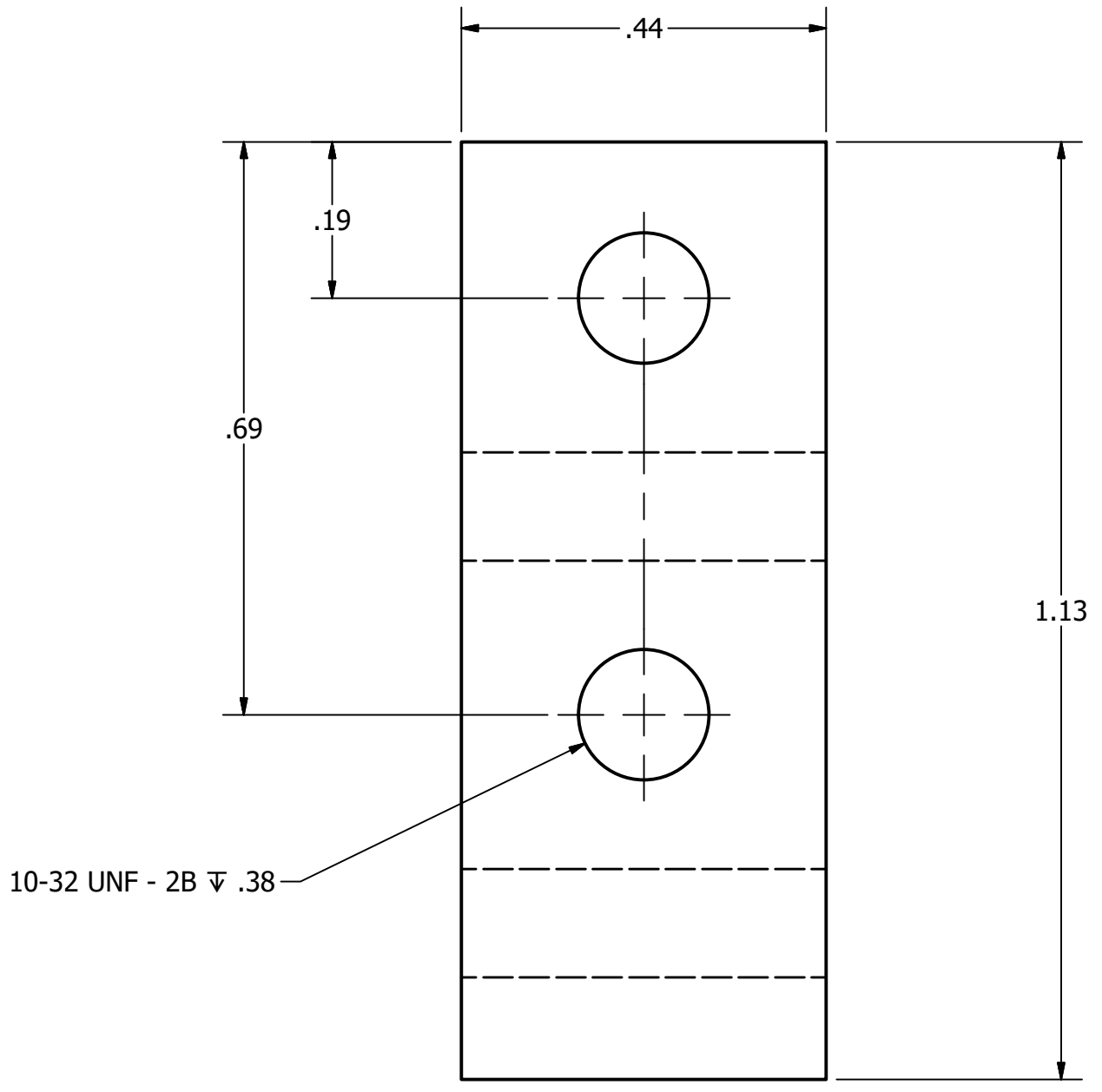


DRAWN Josh	1/4/2018	TITLE		
CHECKED				
QA				
MFG				
APPROVED		SIZE C	DWG NO JP3_Stiffener 3	REV
		SCALE	SHEET 1 OF 1	

4 3 2 1

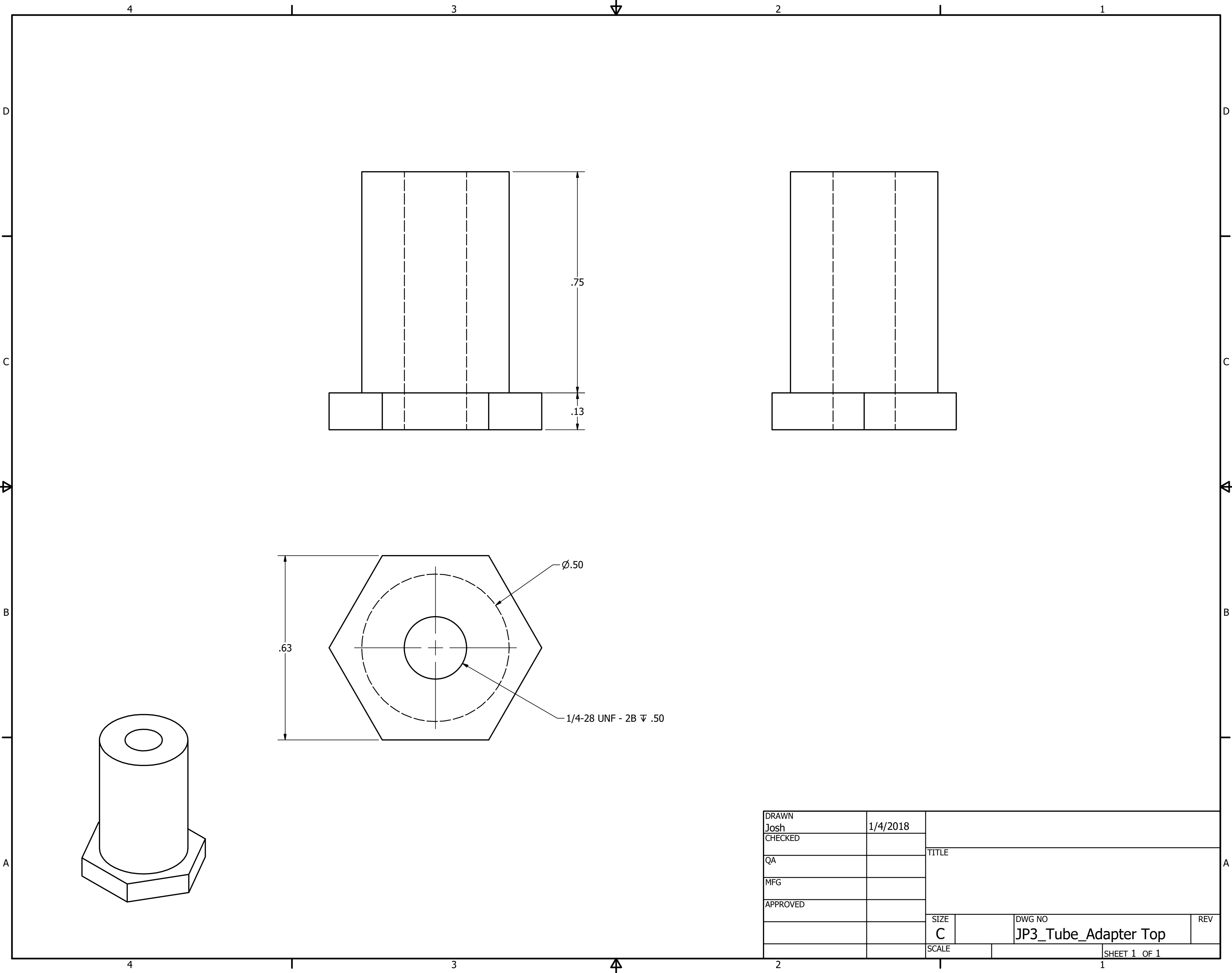
D
C
B
A

D
C
B
A



DRAWN Josh	1/4/2018	TITLE		
CHECKED				
QA				
MFG				
APPROVED		SIZE C	DWG NO jp3_Stiffiner_block	REV
		SCALE	SHEET 1 OF 1	

4 3 2 1



DRAWN Josh	1/4/2018	TITLE		
CHECKED				
QA				
MFG				
APPROVED		SIZE C	DWG NO JP3_Tube_Adapter Top	REV
		SCALE	SHEET 1 OF 1	

4

3

2

1

D

D

C

C

B

B

A

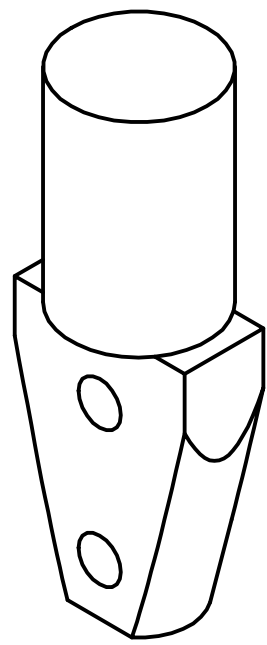
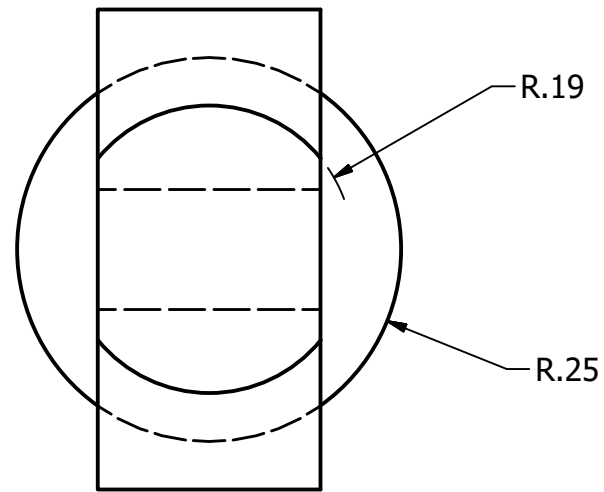
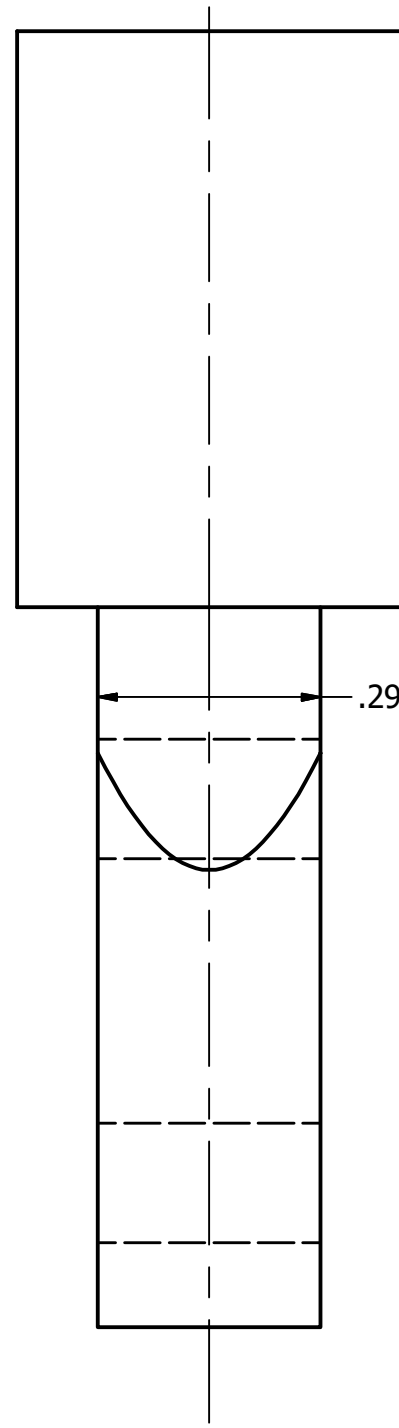
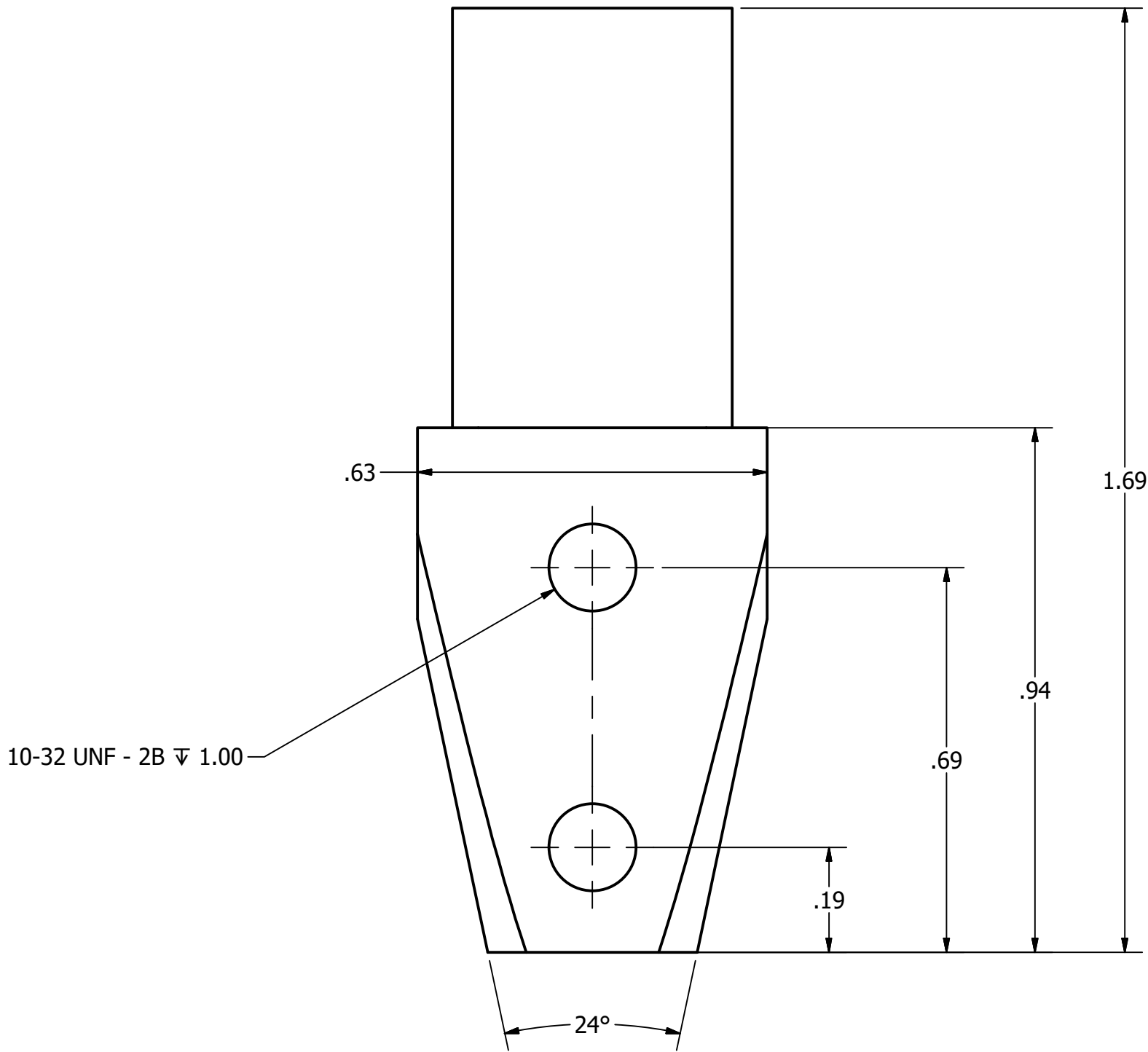
A

4

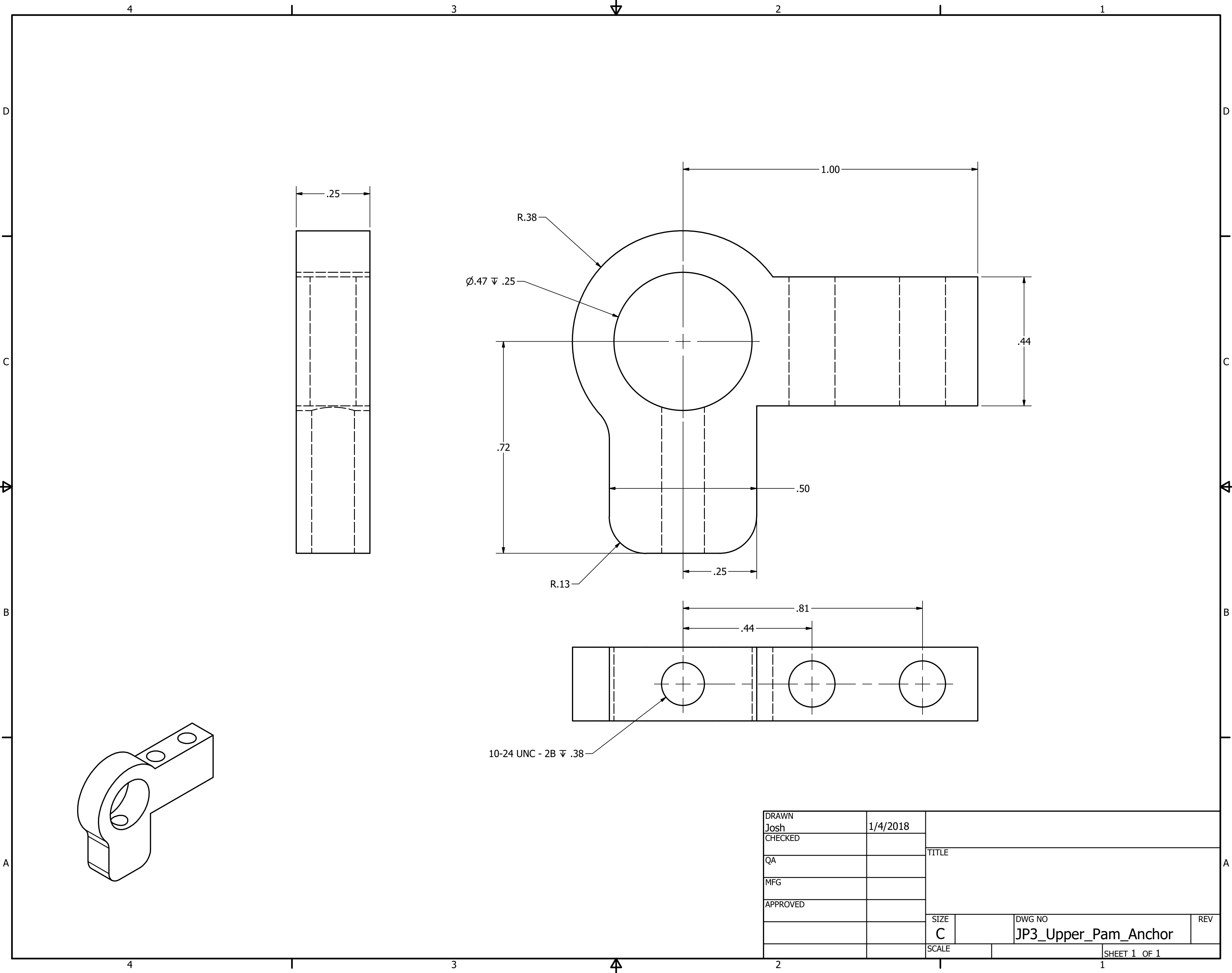
3

2

1



DRAWN Josh	1/4/2018	TITLE		
CHECKED				
QA				
MFG				
APPROVED		SIZE C	DWG NO JP3_Tube_Adapter	REV
		SCALE	SHEET 1 OF 1	

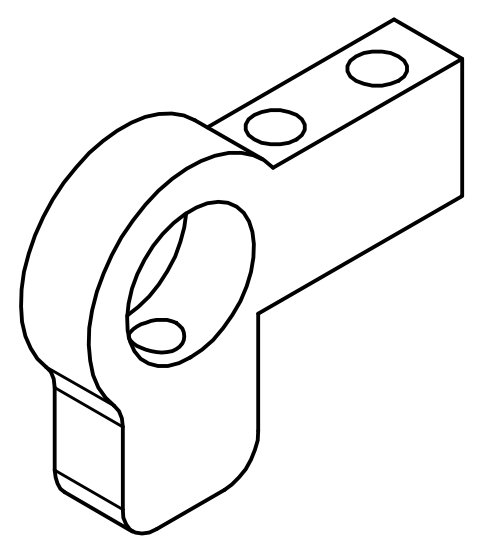


D
C
B
A

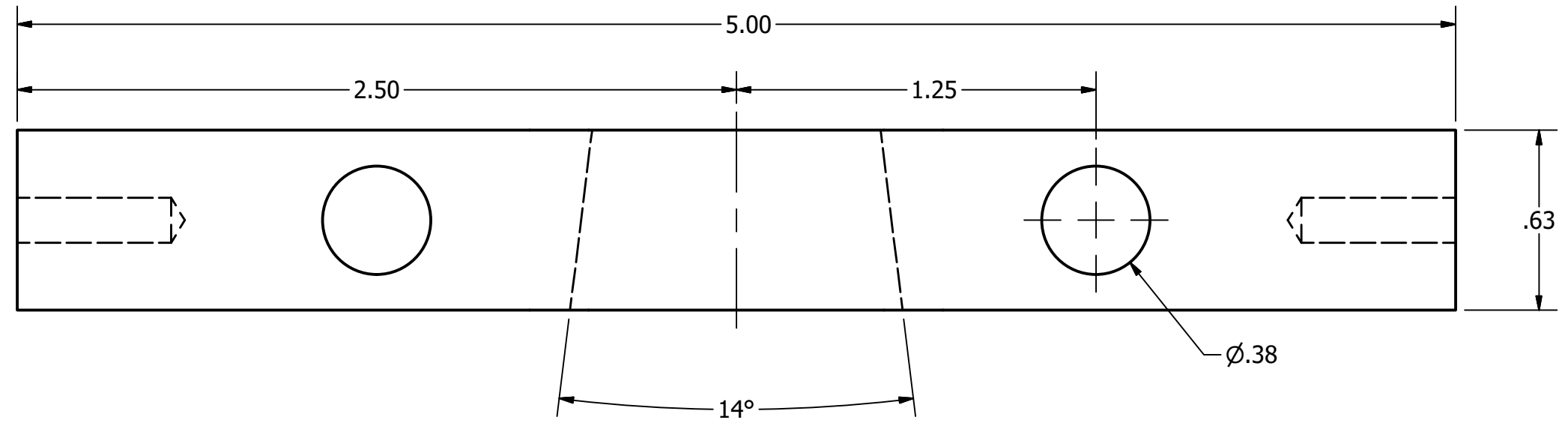
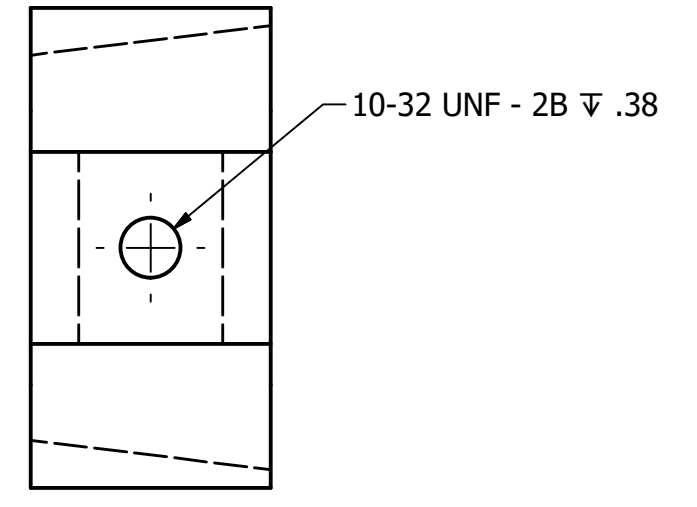
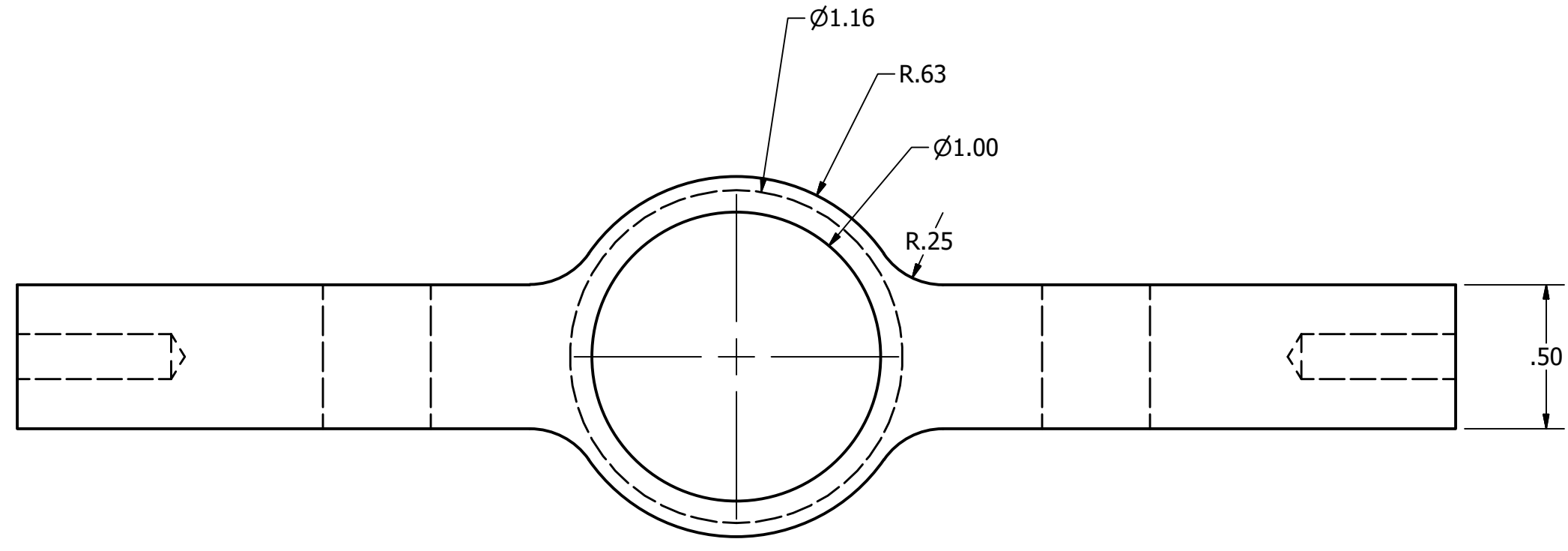
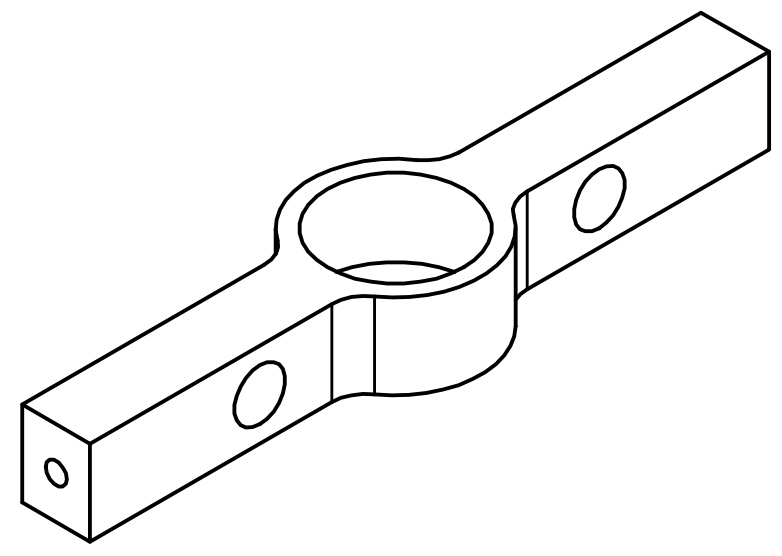
D
C
B
A

4 3 2 1

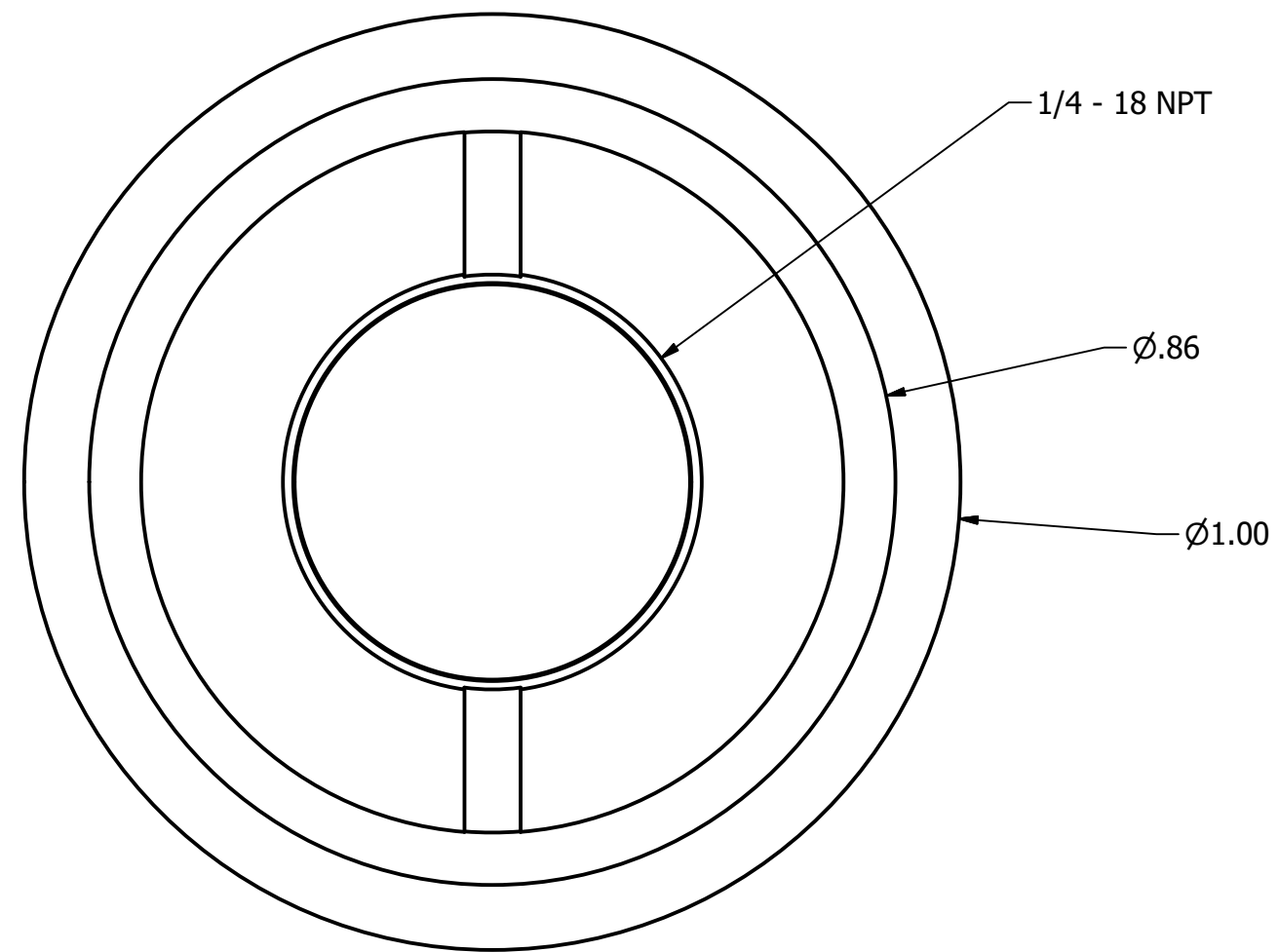
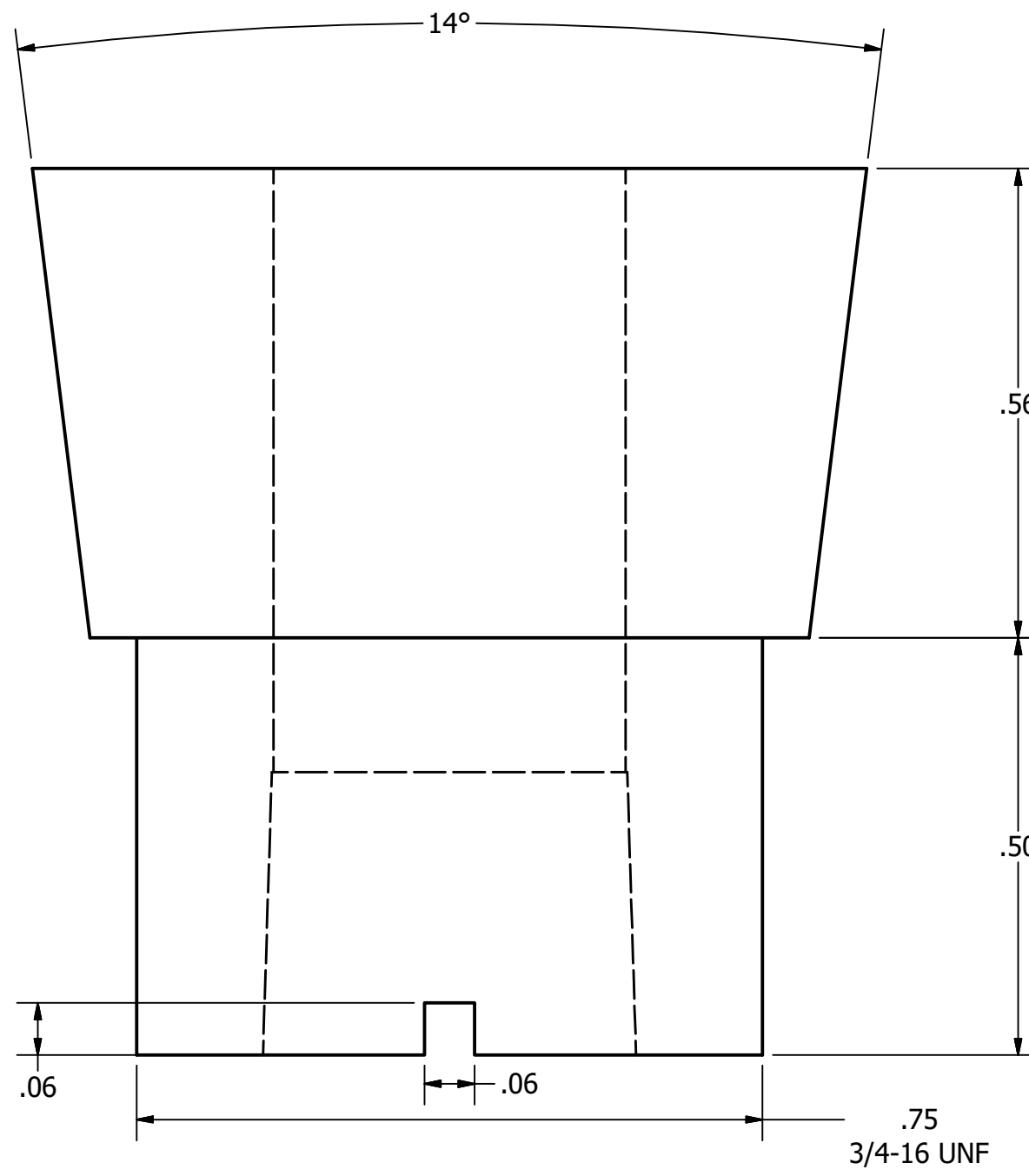
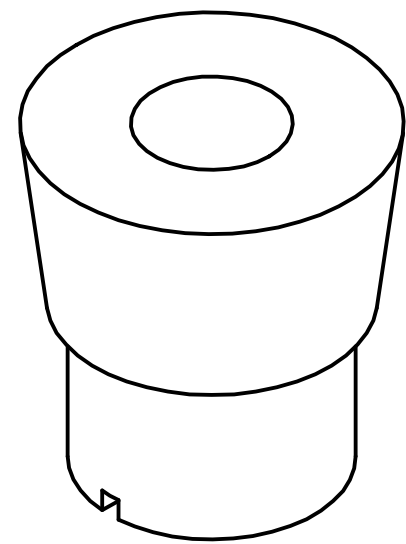
4 3 2 1



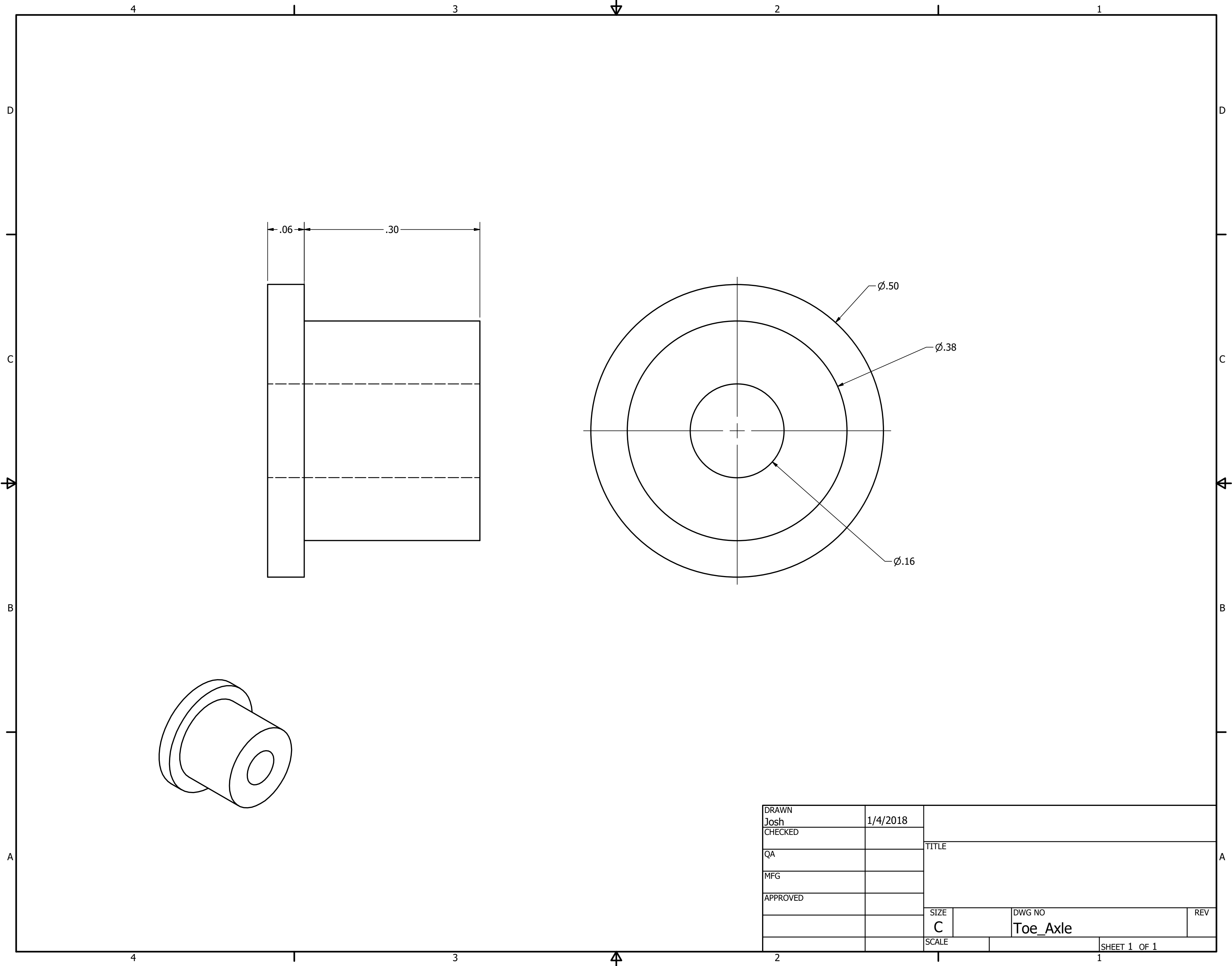
DRAWN Josh	1/4/2018	TITLE		
CHECKED				
QA				
MFG				
APPROVED		SIZE C	DWG NO JP3_Upper_Pam_Anchor	REV
		SCALE	SHEET 1 OF 1	



DRAWN Josh	1/4/2018	TITLE		
CHECKED				
QA				
MFG				
APPROVED		SIZE C	DWG NO LP_compression_sleeve_3	REV
		SCALE	SHEET 1 OF 1	



DRAWN Josh	1/4/2018	TITLE		
CHECKED				
QA				
MFG				
APPROVED		SIZE C	DWG NO LP1_frontcap	REV
		SCALE	SHEET 1 OF 1	



DRAWN Josh	1/4/2018			
CHECKED		TITLE		
QA				
MFG				
APPROVED				
		SIZE C	DWG NO Toe_Axle	REV
		SCALE	SHEET 1 OF 1	

References

- [1] Sawicki, "Mechanical performance of artificial pneumatic muscles to power an ankle-foot orthosis," in *XXth Congress of the International Society of Biomechanics and 29th Annual Meeting of the American Society of Biomechanics*, Cleveland, Ohio, 2006.
- [2] Berkeley Robotics & Human Engineering Laboratory, "HULC," [Online]. Available: <http://bleex.me.berkeley.edu/research/exoskeleton/hulc/>. [Accessed 15 November 2017].
- [3] Army Technology, "Raytheon XOS 2 Exoskeleton," [Online]. Available: <http://www.army-technology.com/projects/raytheon-xos-2-exoskeleton-us/>. [Accessed 15 November 2017].
- [4] M. Philippe, "A Simple Exoskeleton That Assists Plantarflexion Can Reduce the Metabolic Cost of Human Walking," Department of Movement and Sports Sciences, Ghent University, Ghent, Belgium, 2017.
- [5] Humotech, "Humotech - Ankle Exoskeleton," [Online]. Available: <http://www.humotech.com/ankle-exoskeleton/>. [Accessed 15 November 2017].
- [6] G. Sawicki, *Mechanics and energetics of walking with powered exoskeletons*, Ann Arbor, Michigan: University of Michigan, Ann Arbor, 2007.
- [7] K. A. Witte, "Design of Two Lightweight, High-Bandwidth Torque-Controlled Ankle Exoskeletons," in *IEEE International Conference*, 2014.
- [8] L. Mooney, "Biomechanical walking mechanisms underlying the metabolic reduction caused by an autonomous exoskeleton," *Journal of NeuroEngineering and Rehabilitation*, p. 13, 2016.
- [9] Yaskawa Electric, "Yaskawa Electric's Ankle Exoskeleton Gives You Strength," [Online]. Available: <http://crunchwear.com/yaskawa-electrics-ankle-exoskeleton-gives-strength/>. [Accessed 15 November 2017].
- [10] P. Malcolm, "A Simple Exoskeleton That Assists Plantarflexion Can Reduce the Metabolic Cost of Human Walking," *PLOS ONE*, vol. 8, no. 2, 2013.
- [11] U.S. Department of Defense, "Special Operations Develops 'Iron Man' Suit," [Online]. Available:

<https://www.defense.gov/News/Article/Article/604009/>. [Accessed 15 November 2017].

- [12] T. Novacheck, "Biomechanics of Running," University of Minnesota, St. Paul, Minnesota, 1997.
- [13] Y. Muraki, "Joint Torque and Power of the Takeoff Leg in the Long Jump," *International Journal of Sport and Health Science*, vol. 6, no. 2008, pp. 21-32, 2008.
- [14] J. Hoffman, "Norms for Fitness Performance, and Health," 2006, pp. 98-99.
- [15] C. S. Kothera, "Experimental Characterization," University of Maryland, College Park, MD, 2009.
- [16] J. Murillo, "Design of a Pneumatic Artificial Muscle for Powered Lower Limb Prosthesis," University of Ottawa, Ottawa, Ontario, Canada, 2013.
- [17] Enfield Technologies, "LS-V25s Proportional Pneumatic Control Valve Datasheet," Enfield Technologies, 2014.
- [18] "Feetme, smart digital insoles for walking and running," [Online]. Available: <http://www.feetme.fr/en/index.php>. [Accessed 15 November 2017].
- [19] "Flexiforce Pressure Sensor - 25 lb," Sparkfun, [Online]. Available: <https://www.sparkfun.com/products/11207>. [Accessed 15 November 2017].
- [20] "Phidgets Flexiforce Adapter - Robotshop," [Online]. Available: <http://www.robotshop.com/en/phidgets-flexiforce-adapter.html>. [Accessed 15 November 2017].
- [21] The Measurements Group, "Index: Strain Gauge Based Transducers," [Online]. Available: <https://www.thermofisher.com.au/Uploads/file/Environmental-Industrial/Process-Monitoring-Industrial-Instruments/Sound-Vibration-Stress-Monitoring/Stress-Analysis/VishayMM/technology/technotes/Strain-Gauge-Based-Transducers.pdf>. [Accessed 15 November 2017].
- [22] Sparkfun, "Load Sensor - 50 kg," [Online]. Available: <https://www.sparkfun.com/products/10245>. [Accessed 15 November 2017].
- [23] Analog Devices, "AD8426 Wide Supply Range, Rail-to-Rail Output Instrumentation Amplifier," Analog Devices, Inc., Norwood, MA, 2011.

- [24] Robotshop, "Strain Gauge / Instrument Amplifier Shield, Revision 1.2," Robotshop, 2016.
- [25] Fairchild Semiconductor, "BSS138 N-Channel Logic Level Enhancement Mode Field Effect Transistor," Fairchild Semiconductor Corporation, 2005.
- [26] Microchip Technology Inc., "MCP4725 12-Bit Digital-to-Analog Converter with EEPROM Memory in SOT-23-6," Microchip Technology Inc., 2009.